Earth-Science Reviews 267 (2025) 105164

Contents lists available at ScienceDirect

Earth-Science Reviews

journal homepage: www.elsevier.com/locate/earscirev

Review Article

Applications of light hydrocarbons in petroleum geochemistry:A review

Donglin Zhang [a,b,c], Meijun Li [a,b,c,*], Rongzhen Qiao [a,b,c]

[a] Hainan Institute of China University of Petroleum (Beijing), Sanya, Hainan 572025, China
[b] State Key Laboratory of Petroleum Resources and Engineering, China University of Petroleum (Beijing), Beijing 102249, China
[c] College of Geosciences, China University of Petroleum (Beijing), Beijing 102249, China

ARTICLE INFO

Keywords:
Light hydrocarbons
Isotopes
Origins
Maturity
Secondary alteration
Migration

ABSTRACT

Light hydrocarbons are key components of petroleum and contain a wealth of geochemical information. This review provides a comprehensive summary and comments on the research that has been carried out on light hydrocarbons over the past 50 years. It evaluates the applicability and reliability of the various parameters and diagrams that relate to the light hydrocarbons in petroleum from basins worldwide. The chemical compositions and stable isotope values of light hydrocarbons are valuable for identifying the sources and origins of hydrocarbons, their depositional environments, and the maturity of their corresponding source rocks. In addition to thermochemical sulfate reduction, light hydrocarbon parameters are widely used to identify secondary alteration processes, including evaporative fractionation, water washing, biodegradation, and oil cracking. Light hydrocarbon parameters are more effective for tracing natural gas migration than they are for tracing oil migration. Using current light hydrocarbon parameters to accurately identify contributions of petroleum with mixed origins or overlapping secondary effects remains challenging. These challenges may be addressed by using advanced analytical techniques, such as position-specific isotope and clumped isotope analyses combined with other cutting-edge technologies. Advances in separation techniques, high-resolution mass spectrometry, and isotope analysis have significantly enhanced the accuracy of analyzing the chemical and isotopic compositions of light hydrocarbons, providing a deeper understanding of their formation and transformation at microscales.

Contents

* Corresponda2ing author at: China University of Petroleum (Beijing), 18 Fuxue Road, Changping, Beijing 102249, China.
E-mail address: meijunli@cup.edu.cn (M. Li).

https://doi.org/10.1016/j.earscirev.2025.105164
Received 3 March 2025; Received in revised form 12 May 2025; Accepted 12 May 2025
Available online 15 May 2025

1. Introduction

Light hydrocarbons (LHs) are significant components of petroleum. However, they are inconsistently defined in the literature. Dai (1992) defined LHs as compounds with boiling points below 200 °C and molecular carbon numbers between 5 and 10. Mango (1997) classified them as C_1-C_9 hydrocarbons formed at temperatures of approximately 75 °C to 140 °C. Subsequent studies have suggested that LHs are intermediates and catalytic products that are generated during the conversion of oils into natural gas under natural conditions (Mango, 2000). Thermal simulation experiments indicate that C_1-C_{13} fractions and tar pitch are produced by the thermal cracking of C_{14}^{+} fractions in oil (Ungerer et al., 1988). During this process, the formation and cracking of hydrocarbons exhibit considerable overlap (Hill et al., 2003; Ungerer et al., 1988). Researchers are increasingly defining LHs as hydrocarbon compounds with carbon numbers 1–13 (Chang et al., 2017; Hill et al., 2003; Odden et al., 1998; Huang et al., 2022). LHs can be classified into vapor-phase hydrocarbons (C_1-C_5) and liquid-phase hydrocarbons (C_6-C_{13}) according to their phase state (Qiao and Chen, 2022; Behar et al., 1991). Structurally, LHs can be categorized into four groups: *n*-paraffins, isoparaffins, cycloalkanes, and aromatics (Mango, 1997).

Previous studies have shown that the proportion of LHs in conventional oil exceeds 30 %, but can reach up to 90 % in light oil and condensate (Hunt et al., 1980). A biomarker is a complex molecular fossil derived from the biochemical constituents, particularly ester compounds, of once-living organisms. It retains rich geochemical information and is widely used in oil-source correlation, depositional environments reconstruction, thermal maturity assessment, and secondary alterations identification (Chen et al., 1996; Peters et al., 1996; Qiao et al., 2025a). In most light oils and condensates, traditional biomarkers are significantly decreased in their concentrations due to high thermal maturity and secondary alteration processes (Cai et al., 2022; Qiao et al., 2024a; Zhang et al., 2024). In contrast, abundant LHs can potentially serve as effective substitutes, providing richer and more accurate geochemical information. In recent years, the petroleum industry has progressively expanded into unconventional (shale oil and shale gas) and ultra-deep fields, driven by the development of the global energy industry and increasing production demands. Deep and ultra-deep oil is mostly high-maturity light oil and condensate (Dzou and Hughes, 1993; Zhang et al., 2024). These oils have undergone a complex geological evolution and have experienced various secondary alteration processes (Qiao et al., 2024a). Under these conditions, some biomarkers inevitably lose their effectiveness for providing geochemical information as their concentrations decrease significantly (Farrimond et al., 1998). In contrast, LHs remain abundant and are essential for characterizing the geochemical properties of highly mature oil.

Research on LHs began in the 1940s (Forziati et al., 1944). Currently, there are three main schools of thought regarding the genetic mechanisms of LHs. Early studies proposed that LHs in shallow layers were directly inherited from original living matter or formed during the early transformation of sediments (Tissot et al., 1971). LHs primarily originate from the thermal degradation of organic matter when burial depths exceed 1000 m and temperatures exceed 50 °C (Tissot et al., 1971), a view that is supported by the detection of LHs in modern sediments (Hunt et al., 1980; Hunt, 1975). Another view suggests that LHs are transition products formed during the cracking of oil into natural gas (Mango, 2000). In addition, the consistency of the ratios between isomers of LHs suggests that catalysis of transition metals or clay minerals may also contribute to the generation of LHs (Mango, 1987; ten Haven, 1996). The biogenic mechanism must be considered if LHs are defined as organic hydrocarbon compounds with carbon numbers ranging from 1 to 13. Specifically, LHs are produced by anaerobic bacteria decomposing organic matter at low temperatures (Rosenfeld and Silvermann, 1959). All three mechanisms can contribute to LHs formation in oil and gas. Geological conditions dictate which mechanism predominantly controls LHs formation.

LH parameters and isotopic compositions are extensively applied to determine petroleum geochemical characteristics, although their formation mechanisms are still debated. Their applications include identifying the organic matter sources and depositional environments of their corresponding source rocks (Odden et al., 1998; Mango, 1997; Dai, 1992; ten Haven, 1996), evaluating maturity (Hou et al., 1989; Hartgers et al., 1994; Thompson, 1983), correlating oil-gas sources (Halpern, 1995; Chang et al., 2018), identifying secondary alteration processes (Thompson, 1987; Halpern, 1995; George et al., 2002), and tracing hydrocarbon migration direction (Wu et al., 2024a; Chen et al., 2010; Li et al., 2007). Most LH diagrams have limitations, as they are based on data from a limited number of petroliferous basins or petroleum fields (Hu et al., 1990; Halpern, 1995; ten Haven, 1996; Dzou, 2010; Kotarba and Lewan, 2013; Wang et al., 2024a). A comprehensive summary and evaluation of LHs' application in petroleum geochemistry is therefore essential, particularly with recent advancements in analytical techniques such as position-specific isotope and cluster isotope analysis.

In this paper, data on the isotopic and chemical compositions of LHs in petroleum samples from petroliferous basins worldwide are collected and analyzed. The paper summarizes and evaluates the applications and

limitations of LH parameters and diagrams in petroleum geochemical analysis. The aim is to establish LHs as a reliable tool for studying the geochemical characteristics of petroleum, with significant implications for global energy exploration.

2. Method for analyzing LHs

2.1. Molecular compounds

2.1.1. GC

Gas chromatography (GC) is the predominant method for identifying LHs, although pretreatment methods for low molecular weight hydrocarbons in source rocks, natural gas, and oil vary (Schaeffer et al., 1978; Thompson, 1979; Tian et al., 2023). GC was first successfully validated experimentally by James and Martin (1952), who achieved efficient separation of volatile organic compounds. The basic principle is exploiting the differences in the physical properties of compounds, particularly their boiling points, to separate and analyze the components of a mixture.

The isomers in LHs with higher carbon numbers frequently co-elute during boiling-point-based separation, which hinders accurate qualitative and quantitative characterization of the compounds (Wang et al., 2012; Rabbani et al., 2023; Whiticar and Snowdon, 1999). Previous studies have, therefore, concentrated on low-carbon compounds (C_1-C_7) (Cheng et al., 2015a; Wang et al., 2014). C_1-C_5 compounds are primarily applied in gas geochemical studies, whereas C_5-C_7 compounds are commonly utilized in oil characterization (Milkov and Etiope, 2018; Mango, 1997; Halpern, 1995; Thompson, 1979). To date, relatively limited attention has been given to the high-carbon compounds of C_8-C_{13}.

2.1.2. GC × GC-TOFMS

Comprehensive two-dimensional gas chromatography (GC × GC) is an advanced analytical technique that emerged in the early 1990s (Liu and Phillips, 1991). This system utilizes two independent chromatographic columns with orthogonal separation mechanisms, which are connected by a modulator (Bahaghighat et al., 2019). The one-dimensional column is usually a non- or weakly-polar column that separates compounds primarily according to their volatility. The eluates separated by the one-dimensional column are concentrated and aggregated in the modulator, then released in pulses to the two-dimensional column for further separation. The two-dimensional column is typically polar, enabling further separation of compounds based on polarity, thus achieving orthogonal separation (Phillips and Beens, 1999). This significantly enhances the efficiency of separating LHs.

Traditional quadrupole mass spectrometers cannot accommodate the requirements of GC × GC analysis as they are limited by acquisition speed and capacity. Time-of-flight mass spectrometry (TOFMS) is an improved technique that has become prominent since its introduction in the 1990s (Dallüge et al., 2002). This involves using ions with the same kinetic energy but different mass-to-charge ratios (m/z), which travel through a constant electric field at different rates. A substance's composition or structure can, therefore, be determined by measurement of their time (Tranchida et al., 2022). The technology theoretically offers an unlimited mass range, rapid response times, and high sensitivity, facilitating precise analysis of the fragment peaks generated by GC × GC and accurate mass spectrometric evaluations (Aguiar et al., 2010).

The excellent separation capability of GC × GC technology, coupled with the qualitative identification function of TOFMS, addresses the challenges of accurately determining the qualitative and quantitative compositions of complex LHs (Meng et al., 2024, 2025; Cheng et al.,

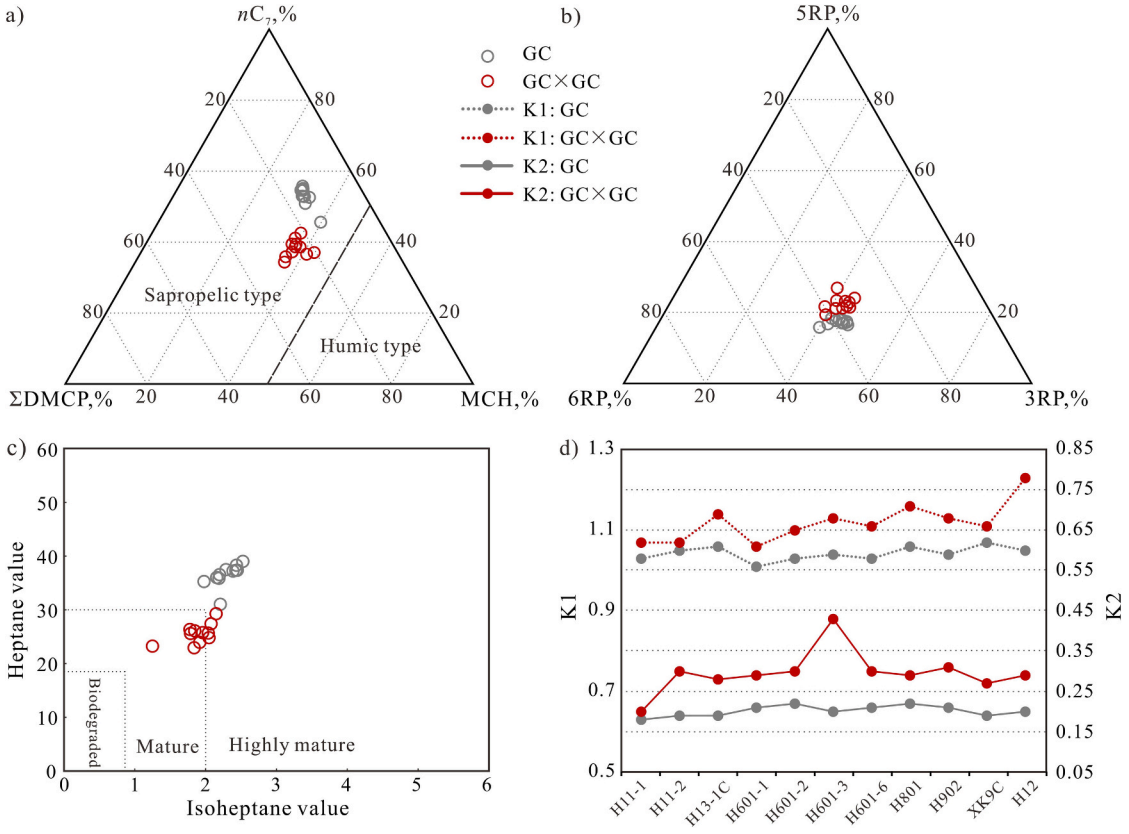

Fig. 1. Comparison of light hydrocarbon parameters using GC × GC and GC. (a) Ternary diagrams showing the relative normalized abundance of nC_7 (nC_7: *n*-heptane), ∑DMCP (DMCP: dimethylcyclopentane), and MCH (MCH: methylcyclohexane) (modified from Hu et al., 1990). (b) Ternary diagrams showing the relative normalized abundance of 5RP, 6RP, and 3RP (RP: ring preference) (modified from ten Haven, 1996). (c) Diagrams of heptane value versus isoheptane value (modified from Thompson, 1983). (d) Line chart of K1 and K2. (Data from Wang et al., 2015a).

2015a). For instance, Wang et al. (2014) and Cheng et al. (2015a) employed GC × GC-TOFMS to identify C_9-C_{10} LHs. This has promoted the further development and application of LHs with higher carbon numbers. The technique has also yielded promising results in the precise identification of alkylbenzenes and diamondoids (Cheng et al., 2015b; Meng et al., 2024, 2025; Zhu et al., 2013; Zhu et al., 2021a; Wang et al., 2013).

2.1.3. Effects of different separation methods on LHs parameters

The occurrence of co-elution in the traditional GC separation process creates compound peak areas that are inaccurate, which affects calculation of the related LH parameters. The orthogonal two-dimensional separation of the GC × GC method reduces co-eluting peaks, enhancing the reliability of the LHs parameter. Wang et al. (2012) employed the GC × GC method to analyze 22 condensate samples from the Sichuan Basin, identifying 67 compounds within the C_3–C_8 range, 13 more than had been detected by GC. Wang et al. (2015a) conducted traditional GC analysis on Ordovician oil from the Halahatang Sag, Tarim Basin, identifying around nine co-elution peaks in the C_5–C_8 range. In contrast, GC × GC enables complete separation of co-eluting compounds.

To directly compare the LH parameters derived from GC and GC × GC methods, LH data were collected from Ordovician oil in the Halahatang Sag, Tarim Basin that had been analyzed using both methods. Fig. 1a demonstrates that the C_7 parameter obtained using GC × GC contains a higher proportion of cycloalkanes than that obtained using GC. This is likely due to the co-elution of cycloalkanes with alkanes in GC, such as 1, cis-2, 2-dimethylcyclopentane with methylcyclohexane (MCH) and ethylcyclopentane (ECP) with 2, 5-dimethylhexane (2, 5DMH). These compounds are fully separated in GC × GC, resulting in an increased detected cycloalkane content in the C_7 fraction. Fig. 1b presents a triangular diagram of the C_7 ring preference (RP). GC × GC detects slightly higher dimethylcyclopentane (DMCP) levels, making its RP calculation more favorable to 5RP than GC. In Fig. 1c, the heptane (H) and isoheptane values (I) calculated by GC are higher than those obtained by GC × GC. In some oil samples, maturity identification results differ between the two methods. This discrepancy may be attributed to the co-elution of 3-ethylpentane (3EP) and 2, 2, 4-trimethylpentane (2, 2, 4TMP) with other compounds in GC, leading to inaccurate compound peak areas. Fig. 1d shows that the K1 and K2 values derived from GC × GC are slightly higher than those obtained by GC. This may result from the co-elution of 1, 2DMCP, 2, 3-dimethylpentane (2, 3DMP), 2-methylhexane (2MH), and 3EP in GC (Wang et al., 2015a).

The differences in LHs parameters derived from GC and GC × GC methods have little effect on the identification of depositional environments and organic matter sources, so the conclusions from both methods are generally accurate (Fig. 1a and b). There are significant discrepancies in H and I value between the two methods, but for other maturity parameters, such as 2, 4DMP and 2, 3DMP, both methods produce similar results (Fig. 1c; Wang et al., 2015a). It is worth noting that the original experimental methods for defining light hydrocarbon parameters were primarily developed using GC. Therefore, caution is warranted when applying GC × GC to derive light hydrocarbon parameters for correlation studies.

2.2. Isotopes

2.2.1. GC-IRMS

In the 1990s, the focus of studies of LHs gradually changed from molecular compounds to compound-specific isotopes with the development of gas chromatography-isotope ratio mass spectrometry (GC-IRMS) online analysis and testing technology (Hayes et al., 1990; Dai and Li, 1994; Whiticar, 1999). GC-IRMS technology enables online measurement of the isotopic compositions of individual LHs in oil and natural gas, with commonly analyzed isotopes including hydrogen and carbon (Huang et al., 2017; Deng et al., 2023; Xiong and Geng, 2000; Wang et al., 2024b). The principle involves converting the sample to a gas, measuring relative isotopic abundances based on differences in mass, and processing the results to obtain an isotope ratio, typically expressed as the δ value. This method further expands the application of LHs in petroleum research.

The isotopes of individual LHs exhibit a strong parental genetic influence and are less impacted by secondary processes than their molecular concentrations. The isotopes can be used for identifying the depositional environments of their corresponding source rocks and carrying out oil-oil and oil-gas correlations (Huang et al., 2022; Bjorøy et al., 1994). Furthermore, the parameters of LH molecules are influenced by the relative contents of compounds, whereas compound-specific isotopes are less affected, so that they more accurately reflect the geochemical information carried by LHs.

2.2.2. PSIA

Position-specific isotope analysis (PSIA) is used to determine stable carbon isotopic compositions at specific atomic positions within a molecule (Abelson and Hoering, 1961). The method dates back to 1961, when Abelson and Hoering (1961) measured position-specific isotopes in amino acid molecules. However, the development of PSIA went through a hiatus due to technological and methodological limitations. It was not until Corso and Brenna (1997) employed gas chromatography-pyrolysis-gas chromatography-isotope ratio mass spectrometry (GC-Py-GC-IRMS) that the online testing of position-specific isotopes was successfully achieved, marking the beginning of a period of rapid development for PSIA. Currently, the primary methods used for PSIA include quantitative nuclear magnetic resonance (NMR) (Gilbert et al., 2013; Liu et al., 2018b; Li et al., 2021), GC-Py-GC-IRMS (Gilbert et al., 2016; Piasecki et al., 2016a; Li et al., 2018a), enzyme-catalyzed reactions (Gao et al., 2016), and the newly developed high-resolution IRMS (Piasecki et al., 2018).

Propane is the primary target for the PSIA of LHs. It is the simplest alkane, composed of one secondary methylene group (-CH_2-) and two primary methyl groups (-CH_3) linked together, with an unequal number of carbon and hydrogen atoms in its structure (Li et al., 2021). Recent research has also explored the position-specific isotopes of butane (C_4) isomers, including *n*-butane (*n*C_4) and isobutane (*i*C_4) (Li et al., 2023; Julien et al., 2020). PSIA reveals details that are often overlooked by conventional "bulk" carbon isotope analysis, capturing isotopic variations within functional groups during and after molecular formation. The method offers significant potential for investigating the temperatures, processes, and pathways involved in natural gas formation (Zhao et al., 2020; Gilbert et al., 2016; Liu et al., 2023).

2.2.3. Clumped isotope

A cluster isotope is a multiply-substituted isotopologue that contains two or more heavy isotopes (rare isotopes), and its value represents the

Table 1
Relative abundances and masses of the isotopologues of methane (form Stolper et al., 2014).

Cardinal mass	Isotopologue	Proportional relative abundance of CH_4*	Exact mass (amu)
16	$^{12}CH_4$	9.88×10^{-1}	16.031
17	$^{13}CH_4$	1.11×10^{-2}	17.035
	$^{12}CH_3D$	6.16×10^{-4}	17.038
18	$^{13}CH_3D$	6.92×10^{-4}	18.041
	$^{12}CH_2D_2$	1.44×10^{-7}	18.044
19	$^{13}CH_2D_2$	1.62×10^{-9}	19.047
	$^{12}CHD_3$	1.49×10^{-11}	19.050
20	$^{13}CHD_3$	1.68×10^{-13}	20.053
	$^{12}CD_4$	5.82×10^{-16}	20.056
21	$^{13}CD_4$	6.54×10^{-18}	21.060

* Assumes that isotopes are randomly distributed throughout all isotopologues and that $\delta^{13}C = 0$ ‰ and $\delta D = 0$ ‰ (relative to VPDB and VSMOW respectively).

extent to which the isotopologue's relative abundance deviates from a random distribution (Eiler, 2007; Henkes et al., 2018; Douglas et al., 2017). This isotopic analysis technique was initially proposed for the paleotemperature reconstruction of carbonate minerals in 2004 (Eiler and Schauble, 2004). However, it was not until 2007 that Eiler summarized the methods, principles, and concepts of the method (Eiler, 2007; Eiler and Schauble, 2004). The method is primarily used to measure the total concentrations of isotopologue molecules containing multiple heavy isotope atoms. In methane (C_1), there are 10 isotopologues with cardinal masses ranging from 16 to 21 (Table 1). Two high-resolution isotope mass spectrometers—the MAT 253 Ultra (Thermo Scientific) and the Panorama (Cameca Limited)—are widely used to analyze the methane clumped isotope. The MAT 253 Ultra achieves a resolution of 27,000, while the Panorama reaches 40,000 (Young et al., 2016; Eiler, 2013). Both instruments are used to measure the combined concentrations of $^{13}CH_3D$ and $^{12}CH_2D_2$, commonly expressed as Δ18.

Samples for testing must have a relative purity exceeding 99 %. Sample pretreatment, therefore, plays a crucial role. Stolper et al. (2014) developed techniques for concentrating and purifying methane without inducing isotope fractionation. These methods enable the separation of methane from natural gas, meeting the requirements for cluster isotope analysis. In addition, studies on ethane (C_2) and propane (C_3) cluster isotopes have also been reported (Xia and Gao, 2024; Yin et al., 2024; Clog et al., 2018).

3. Stability of light hydrocarbons

Due to their low molecular weights and boiling points, LHs are prone to evaporation, which significantly affects their concentrations and distributions. Natural gas samples are typically collected using pressurized cylinders. The sealing and stability of the cylinder prevents evaporation of the gas contents. In contrast, oil is usually collected and stored in glass bottles, which offer inferior sealing and stability compared to pressurized cylinders. As a result, LH components are subject to loss during oil sample transportation and storage.

Cañipa-Morales et al. (2003) demonstrated that the evaporation of LHs is closely related to their boiling points. Compounds with lower boiling points, such as 2, 2DMP and 2, 4DMP, evaporate more rapidly. In contrast, compounds with higher boiling points, such as *n*-heptane (nC_7) and MCH, evaporate more slowly, resulting in increased relative concentrations. Xiao et al. (2012) determined that molecular weight and chemical structure significantly influence the evaporation of C_5-C_8 LHs. Compounds with greater molecular weights and more complex chemical structures are more stable. This uneven loss of LHs during evaporation causes "distortion" of the related parameters. For instance, the calculated oil generation temperature and the K2 value of evaporated oil samples are generally lower than those of the original oil (Cañipa-Morales et al., 2003).

Evaporation also affects the carbon isotopes ($\delta^{13}C$) of LHs. Bjorøy et al. (1994) placed oil in an open beaker to evaporate naturally and monitored the changes in *n*-paraffins, isoparaffins, cycloalkanes, and aromatics over 48 h. They found that the variation in $\delta^{13}C$ was mostly less than 1 ‰. The isotope effect on C_4–C_{14} LHs during storage is, therefore, minimal. Xiao et al. (2012) examined the $\delta^{13}C$ changes in individual C_5–C_8 LHs during natural evaporation. They found that when the evaporative loss of individual compounds is less than 70 %, the $\delta^{13}C$ change is less than 1.0 ‰. However, when the volatile loss exceeds 70 %, the isotope change exceeds 1.0 ‰. Subsequent studies have shown that carbon isotope fractionation decreases significantly with increasing carbon number during natural evaporation. Additionally, the stability of $\delta^{13}C$ in cycloalkanes is considerably higher than in aromatics, *n*-paraffins, and isoparaffins (Liang et al., 2017; Xiao et al., 2012).

It is crucial to ensure the initial conditions of oil samples before utilizing LHs components and $\delta^{13}C$ to characterize their geochemical properties. If immediate analysis is not feasible, the samples should be stored at low temperatures to minimize LHs component loss and $\delta^{13}C$ fractionation.

4. Genetic types of natural gas

Natural gas is a high-quality fuel composed of minor amounts of non-hydrocarbon gas and low-molecular-weight hydrocarbons. Its origins can be further classified into microbial, abiogenic, and thermogenic processes (Faramawy et al., 2016). Although a biogenic gas has been proved to exist, no commercially viable a biogenic gas fields have yet to be identified. Commercially valuable gas fields typically consist of microbial gas derived from microbial activity or thermogenic gas generated by thermal cracking (Rice, 1992; Rice and Claypool, 1981; Katz et al., 2002; Katz, 2011). Natural gas is classified into abiogenic gas, secondary microbial gas, primary microbial gas-F (methyl-type fermentation), primary microbial gas-CR (carbon dioxide reduction), biogenic gas, humic-type gas, oil-cracking gas (sapropelic-type gas), kerogen-cracking gas (sapropelic-type gas), and mixed gases of multiple origins. It is notable that some unconventional gases, shale and coalbed gas, can also come from thermogenic, microbial, or mixed processes (Fig. A. 1; Golding et al., 2013).

Natural gas formed by different genetic mechanisms has different hydrocarbon compositions and different stable isotope characteristics. Many studies have created classification diagrams for different genetic types of natural gas (Xie et al., 2016; Hu et al., 2007; Bernard et al., 1977, 1978; Dai, 1992; Rooney et al., 1995; Jenden et al., 1988; Whiticar, 1999; Milkov and Etiope, 2018).

4.1. Identification of abiogenic gas

Abiogenic gas has garnered widespread attention and has been identified in various geological settings worldwide, including hydrocarbon gases in the hydrothermal fluids at the 21°N mid-ocean ridge in the eastern Pacific (Proskurowski et al., 2008), CH_4 seeps in the Zambales ophiolite in the Philippines (Abrajano et al., 1988), and CH_4 gas columns in ultrabasic rocks along fault zones at 15°20′N on the Mid-Atlantic Ridge (Charlou et al., 1998). Abiogenic gas is typically derived from mantle degassing and Fischer-Tropsch type (FTT) synthesis (Liu et al., 2021). FTT synthesis refers to the catalytic reaction of CO and H_2 to form hydrocarbons under specific temperature and pressure conditions (Lancet and Andets, 1970). Except for methane from Canadian and Scandinavian shield rocks, $\delta^{13}C_1$ values of abiogenic gases are typically greater than −30 ‰ (Dai et al., 2005, 2008; Wang et al., 2009). The endmembers of methane derived from mantle degassing and FTT synthesis typically exhibit $\delta^{13}C_1$ values of −15 ‰ and − 30 ‰, respectively (Liu et al., 2021). Thus, $\delta^{13}C_1$ serves as a key indicator for distinguishing abiogenic gases. Additionally, δD_1 values are commonly used alongside $\delta^{13}C_1$ values to characterize gas origin (Bernard et al., 1978; Milkov and Etiope, 2018; Liu et al., 2019a, 2019b; Zhu et al., 2025). Notably, the $\delta^{13}C_1$ characteristics of abiogenic gas can be covered by those of biogenic gas in sedimentary basins, making them difficult to distinguish, as observed in mixed gases from the Songliao, Bohai Bay, and Subei basins in China (Jiang et al., 2025; Liu et al., 2016, 2021, 2025). Moreover, coal-derived gases from highly mature coal measures (e.g., the Kela 2 gas field in the Kuqa Depression, Tarim Basin) also exhibit high $\delta^{13}C_1$ values (> − 30 ‰), resembling those of abiogenic gases and thereby complicating origin identification (Liu et al., 2021). In such cases, carbon isotope values of methane alone are insufficient to determine the abiogenic gases. However, the helium isotope ratio ($^3He/^4He$) can effectively identify the presence of abiogenic gas. Typically, R/Ra > 0.1 (R and Ra represent the $^3He/^4He$ ratios of the sample and atmosphere, respectively) suggests a mantle-derived helium component (Jenden et al., 1993).

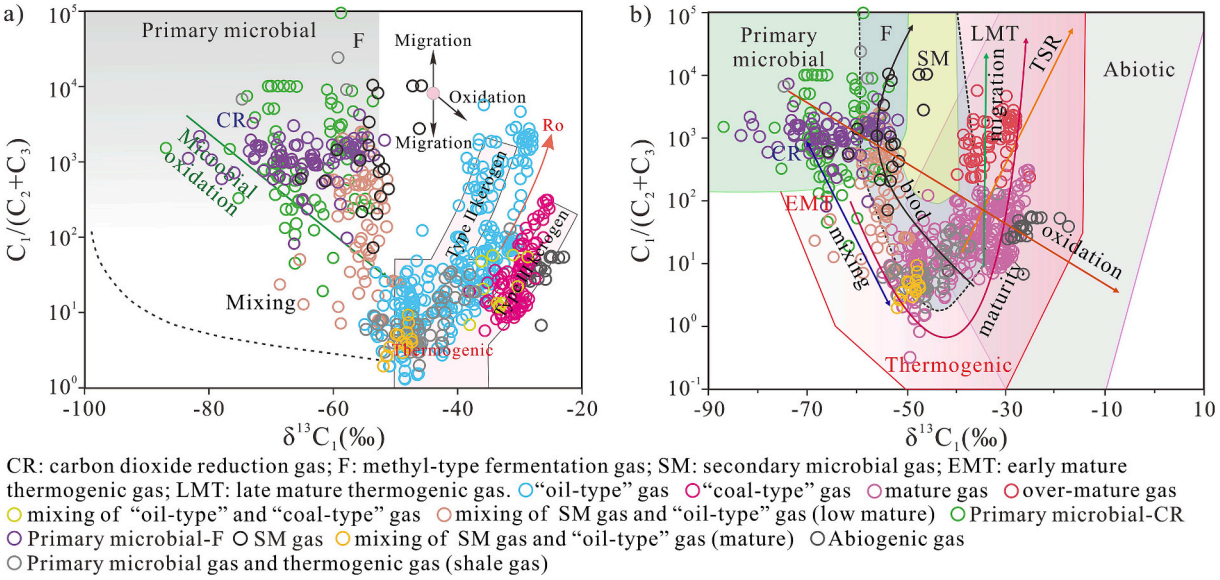

Fig. 2. (a) Diagrams of $\delta^{13}C_1$ versus $C_1/(C_2 + C_3)$ for identifying different types of natural gas (modified from Bernard et al., 1978). (b) Diagrams of $\delta^{13}C_1$ versus $C_1/(C_2 + C_3)$ (modified from Milkov and Etiope, 2018). (For details of the data sources, see Fig. A.1).

4.2. Identification of microbial and thermogenic gases

Microbial gas accounts for more than 20 % of commercially exploitable gas fields, with the remainder consisting predominantly of thermogenic gas (Rice and Claypool, 1981; Shurr and Ridgley, 2002; Katz et al., 2002; Katz, 2011). Exploring and developing these two types of natural gas presents distinct challenges. Microbial gas formation relies on bacterial biodegradation, and bacteria in sedimentary strata cannot survive at temperatures exceeding 88 °C (Stetter et al., 1993; Rice and Claypool, 1981). Consequently, microbial gas exploration and production are generally limited to middle and shallow sedimentary strata, including shallow coalbed and shale gas, which may also be biogenic (Brown, 2011; Golding et al., 2013). In contrast, thermogenic gas forms through the thermal cracking of organic matter, such as oil and kerogen, at temperatures above 65 °C (Schoell, 1983). Many studies have focused on the characterization and differentiation of the geochemical characteristics of these two types of natural gas (Fuex, 1977; Dai, 1992; Whiticar, 1999; Bernard et al., 1977).

Bernard et al. (1977) distinguished thermogenic gas from microbial gas by plotting a diagram that correlated $\delta^{13}C_1$ values with the $C_1/(C_2 + C_3)$ ratio. Microbial gas typically exhibits a $\delta^{13}C_1$ value lower than −55 ‰ and $C_1/(C_2 + C_3)$ exceeding 1000, whereas thermogenic gas is defined by higher concentrations of C_2^+ components and $\delta^{13}C_1$ values between −30 ‰ and − 50 ‰ (Bernard et al., 1977). Mixed gas, which shares characteristics of both microbial and thermogenic origins, falls between these categories. Whiticar (1999) further classified microbial gas into two types based on origin: gas from CO_2-reduction in marine sediments (primary microbial-CR; $\delta^{13}C_1 < -60$ ‰) and gas from methyl-type fermentation in continental deposits (primary microbial-F; $\delta^{13}C_1 > -60$ ‰) (Milkov and Etiope, 2018; Whiticar, 1999). This diagram also clarified other critical elements, such as the boundary between humic-type and sapropelic-type gases and the thermal evolution trend of thermogenic gas (Fig. 2a). The diagram, therefore, demonstrates significant practical utility and has been widely adopted.

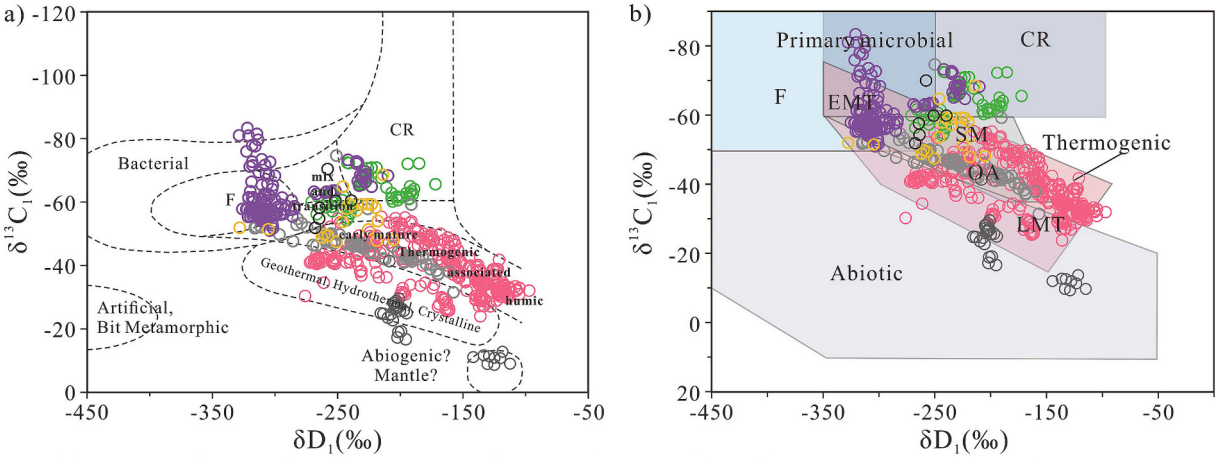

Fig. 3. (a) Diagrams of δD_1 versus $\delta^{13}C_1$ (modified from Whiticar, 1999). (b) Diagrams of δD_1 versus $\delta^{13}C_1$ (modified from Milkov and Etiope, 2018). (For details of the data sources, see Fig. A.2).

When the diagram was first introduced, the microbial gas in the diagram was limited to primary microbial gas, defined as natural gas generated by the microbial decomposition of sedimentary organic matter (Rice, 1992). Secondary microbial gas, produced by the anaerobic biodegradation of petroleum, was initially excluded (Jones et al., 2008). Milkov (2011) reviewed the characteristics of gases in global biodegradation zones, reevaluated the identification criteria for $C_1/(C_2 + C_3)$ ratios and $\delta^{13}C_1$ values, and proposed an area for identifying secondary microbial gas. Milkov's study found that secondary microbial gas constitutes the majority (62.50 %–73.33 %) of microbial gas in sedimentary basins (Milkov, 2011). Secondary microbial gas is primarily produced by oil biodegradation and typically exhibits very low $\delta^{13}C_1$ values (Jones et al., 2008). Subsequent geological processes result in the incorporation of thermogenic gas which produces a broader $\delta^{13}C_1$ distribution, ranging from −55 ‰ to −35 ‰ (Larter and di Primio, 2005).

Milkov and Etiope (2018) revised the $\delta^{13}C_1$ versus $C_1/(C_2 + C_3)$ diagram using data from 13,491 gas samples from around the world, enhancing its accuracy and making it more scientifically interpretable (Fig. 2b). The updated diagram eliminates the differentiation between sapropelic-type and humic-type gases, instead reclassifying thermogenic gas based on its properties at various maturity stages (Fig. 2b). It also incorporates trends related to mixing, thermochemical sulfate reduction (TSR), and migration processes (Fig. 2b). Although the revised diagram cannot distinguish between humic- and sapropelic-type gases, it provides an effective characterization of thermogenic gas maturity stages. For example, natural gas with high thermal evolution from marine strata of the Sichuan Basin is distributed in the late mature thermogenic gas zone (Fig. A. 1b).

Compared to its predecessor, the updated diagram offers a clearer delineation of mixed gas but still shows uncertainties regarding the precise genetics of overlapping regions of the various gases. For example, the primary microbial gas-CR and F in the samples used in this study cannot be effectively distinguished on the diagram (Fig. 2b). The mixed gas (secondary microbial gas and thermogenic gas) and thermogenic gas in the Tahe oilfield (Tarim Basin) are not clearly differentiated (Fig. 2b). The high temperatures and anaerobic conditions in ultra-deep reservoirs are inhospitable to microbial survival and activity (Katz et al., 2002; Katz, 2011). Thus, secondary microbial gases in the Tahe oilfield are likely remnants of paleo-microbial activity from earlier burial stages (Jiang and Liu, 2025).

Whiticar (1999) developed $\delta^{13}C_1$ versus δD_1 diagrams to differentiate among primary microbial gas-CR, primary microbial gas—F, thermogenic gases, and biogenic gas (Fig. 3a). Later, Milkov and Etiope (2018) expanded this diagram by incorporating a secondary microbial gas region (Fig. 3b). While the updated diagram appears to be effective in distinguishing between primary microbial gas-CR and F, in practice it struggles to reliably separate secondary microbial gas, primary microbial gas-CR, and F (Fig. 3b). At present, there is no reliable method for differentiating these types of natural gas, and most studies still distinguish them according to the sources of their organic matter and clear identification of primary microbial gas (Ni et al., 2013).

The $\delta^{13}C_{CO2}$ value was introduced to distinguish between mixed gas (thermogenic gas and secondary microbial gas) and thermogenic gas (Milkov, 2011). A high $\delta^{13}C_{CO2}$ value ($\delta^{13}C_{CO2} > 0$) suggests secondary microbial gas formation via oil biodegradation (Boreham et al., 2001; Milkov, 2011). However, most carbonate carbon isotope values that are unaltered by bioturbation are greater than 0 ‰, and the $\delta^{13}C$ of the decomposed CO_2 exhibits isotopic inheritance (Coudrain-Ribstein et al., 1998; Warren, 2000; Cai et al., 2001). Elevated $\delta^{13}C_{CO2}$ values in carbonate reservoirs can also result from processes such as carbonate decomposition at 10–200 °C (Smith and Ehrenberg, 1989; Coudrain-Ribstein et al., 1998; Cai et al., 2001).

Shale and coalbed gas are natural gases generated in the shale or coal reservoirs. These gases can originate from thermogenic, microbial, or mixed processes. Methane, ethane, carbon dioxide, and nitrogen are the primary components of shale and coalbed gas (Golding et al., 2013).

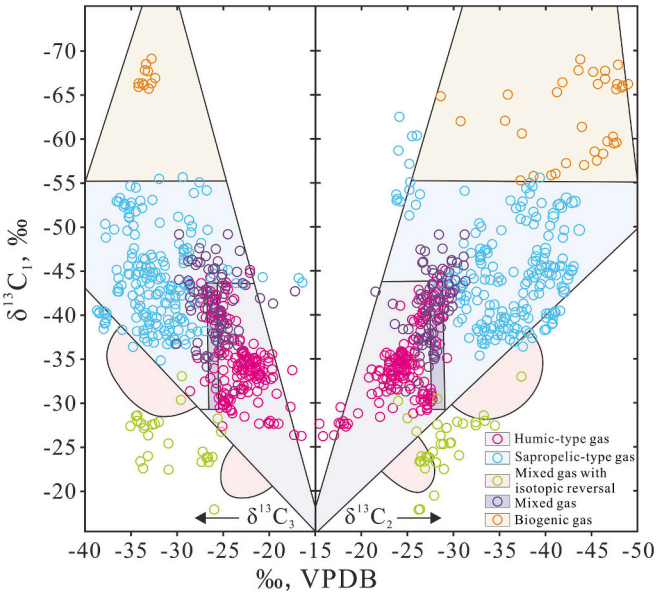

Fig. 4. Genetic identification diagram of natural gas in $\delta^{13}C_1$–$\delta^{13}C_2$–$\delta^{13}C_3$ (modified from Dai, 1992). (For details of the data sources, see Fig. A.3).

Consequently, conventional natural gas genesis identification methods remain valid for assessing the origin of shale and coalbed gas. A key issue is the inversion of carbon isotopes in overly mature shale and coalbed gas (Golding et al., 2013; Peng et al., 2020). Thermal cracking of wet-gas components and potential free radical decomposition or polymerization reactions at high maturity typically results in carbon isotope inversion ($\delta^{13}C_{C2} < \delta^{13}C_{C1} < \delta^{13}C_{C3}$, $\delta^{13}C_{C2} < \delta^{13}C_{C3} < \delta^{13}C_{C1}$, and $\delta^{13}C_{C3} < \delta^{13}C_{C2} < \delta^{13}C_{C1}$) of alkane gases (Cesar et al., 2020; Peng et al., 2020). Carbon isotope inversion can introduce errors in genesis identification results. The inversion of carbon isotopes in the over-mature stage significantly affects the accuracy of natural gas maturity assessments. This issue will be further explored in Section 6.1.

4.3. *Identification of "sapropelic-type" and "humic-type" gases*

Natural gas can be further divided into "humic-type" gas and "sapropelic-type" gas according to the organic matter types (e.g., Type II and III organic matter) of the source rocks (Behar et al., 1995; Schoell, 1980). Stable isotopes of natural gas exhibit significant parental inheritance characteristics, and those derived from different organic precursors during thermal cracking can vary substantially (Whiticar, 1999; Milkov, 2011; Liu et al., 2019a, 2019b). Humic kerogen is enriched in aromatic and heterocyclic compounds and relatively abundant in ^{13}C (Dai, 1992). In contrast, sapropelic kerogen primarily consists of long-chain aliphatic groups and is relatively enriched in ^{12}C (Dai, 1992). The carbon isotopic of natural gas has the characteristics of parent material inheritance (Fuex, 1977; Schoell, 1980; Dai, 1992; Whiticar, 1999; Milkov and Etiope, 2018). Thus, gases formed from humic kerogen exhibit a heavier carbon isotope composition than those derived from sapropelic kerogen at the same degree of thermal evolution. Dai (1992) introduced the $\delta^{13}C_1$-$\delta^{13}C_2$-$\delta^{13}C_3$ crossplot to classify genetic types of natural gas according to the distribution patterns of $\delta^{13}C$ (Fig. 4). In this diagram, $\delta^{13}C_1 = -55$ ‰ is generally recognized as the boundary for differentiating microbial from thermogenic gas (Bernard et al., 1977, 1978). Statistical data indicate that $\delta^{13}C_2 = -28$ ‰ and $\delta^{13}C_3 = -25$ ‰ serve as dividing boundaries for distinguishing humic-type from sapropelic-type gases (Dai, 1992). Typically, humic-type gas is distinguished by $\delta^{13}C_3$ values exceeding −25 ‰ and $\delta^{13}C_2$ values greater than −28 ‰, whereas sapropelic-type gas is identified by $\delta^{13}C_3$ values below −25 ‰ and $\delta^{13}C_2$ values under −28 ‰ (Fig. 4; Dai, 1992).

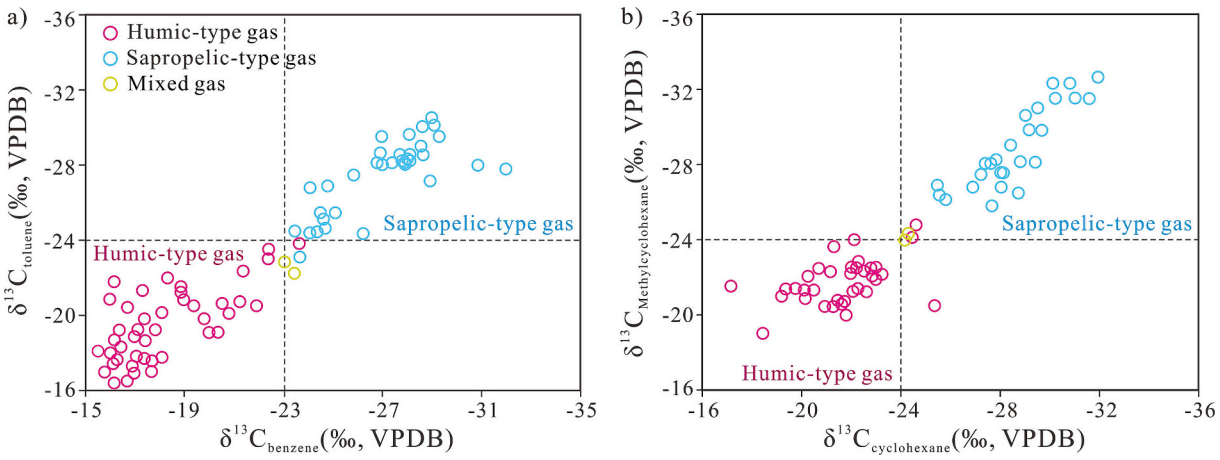

Fig. 5. (a) Diagrams of $\delta^{13}C_{benzene}$ versus $\delta^{13}C_{toluene}$ for identifying genetic types of natural gas (modified from Hu et al., 2007). (b) Diagrams of $\delta^{13}C_{cyclohexane}$ versus $\delta^{13}C_{methylcyclohexane}$ (modified from Hu et al., 2007). (For details of the data sources, see Fig. A.4).

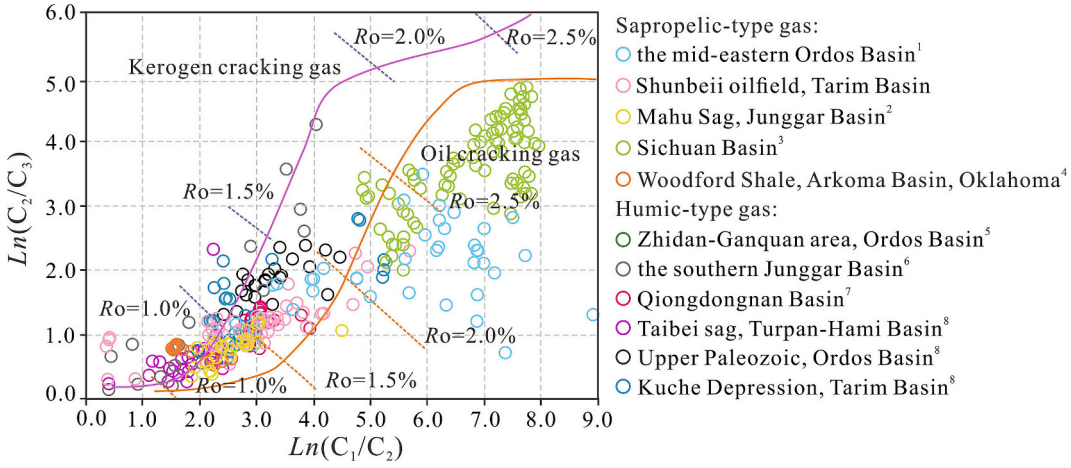

Fig. 6. Diagrams of $Ln(C_1/C_2)$ versus $Ln(C_2/C_3)$ for identifying different types of natural gas (modified from Xie et al., 2016). Data 1 from Yang et al., 2022; 2 from Kang et al., 2021; 3 from Xie et al., 2021; 4 from Liu et al., 2019; 5 from Chen et al., 2020; 6 from Yu et al., 2024; 7 from Liang et al., 2020; and 8 from Wang et al., 2015b.

Based on collected samples, the $\delta^{13}C_1$-$\delta^{13}C_2$-$\delta^{13}C_3$ diagram is generally effective in distinguishing humic-type gas from sapropelic-type gas (Fig. 4). However, in the overlap region between sapropelic- and humic-type gases, the samples cannot be precisely classified (Fig. 4). The inversion of carbon isotopes under complex geological conditions poses significant challenges for genetic identification using this diagram (Fuex, 1977; Liu et al., 2018a; Dai et al., 2004; Coleman et al., 1981).

Early studies indicated that the $\delta^{13}C$ of LHs in natural gas is relatively unaffected by migration and thermal evolution (Jiang et al., 2000). Subsequent research has revealed that the $\delta^{13}C$ of specific LHs, such as methylcyclohexane (MCH), cyclohexane (CH), toluene (Tol), and benzene (Bz), can effectively differentiate humic-type gas from sapropelic-type gas (Tian et al., 2023; Gong et al., 2016; Hu et al., 2007). For sapropelic-type gas, the isotope thresholds are $\delta^{13}C_{Bz} < -23$ ‰, $\delta^{13}C_{Tol} < -24$ ‰, $\delta^{13}C_{CH} < -24$ ‰, and $\delta^{13}C_{MCH} < -24$ ‰. Conversely, humic-type gas exhibits $\delta^{13}C_{Bz} > -23$ ‰, $\delta^{13}C_{Tol} > -24$ ‰, $\delta^{13}C_{CH} > -24$ ‰, and $\delta^{13}C_{MCH} > -24$ ‰ (Fig. 5). Notably, genetic identification diagrams based on $\delta^{13}C_{Bz}$ vs. $\delta^{13}C_{Tol}$ and $\delta^{13}C_{CH}$ vs. $\delta^{13}C_{MCH}$ in LHs outperform the traditional $\delta^{13}C_1$-$\delta^{13}C_2$-$\delta^{13}C_3$ identification diagrams in distinguishing gas types (Figs. 4 and 5).

4.4. Identification of kerogen and oil cracking gases

The compositions and pyrolysis products of type II and type III kerogen differ significantly. Type III kerogen is primarily composed of aromatic and heterocyclic compounds and predominantly produces kerogen cracking gas with negligible oil yields. Conversely, type II kerogen is characterized by an abundance of long-chain aliphatic groups and co-generates substantial amounts of both oil and natural gas during pyrolysis. Type II kerogen source rocks generate sapropelic-type gas by two primary processes: kerogen cracking to kerogen cracking gas and oil thermal cracking to oil cracking gas (Xie et al., 2016; Behar et al., 1992; Prinzhofer et al., 2000).

Behar et al. (1992) observed in a closed-system thermal simulation experiment that C_1 formed at a notably higher rate than C_2 in kerogen cracking gas, while C_2 formed at a rate similar to propane (C_3). In oil cracking gas, C_1 formed at a rate comparable to C_2, whereas C_2 formed at a significantly higher rate than C_3. Based on these results, an $\ln(C_2/C_3)$ vs. $\ln(C_1/C_2)$ crossplot was constructed to distinguish oil cracking gas from kerogen cracking gas (Behar et al., 1992). However, the relatively low thermal evolution in the simulation experiment limited the effectiveness of the diagrams (Prinzhofer and Huc, 1995; Behar et al., 1992). Subsequently, Xie et al. (2016) improved the crossplot by adding additional simulation experiments and refining the criteria for distinguishing

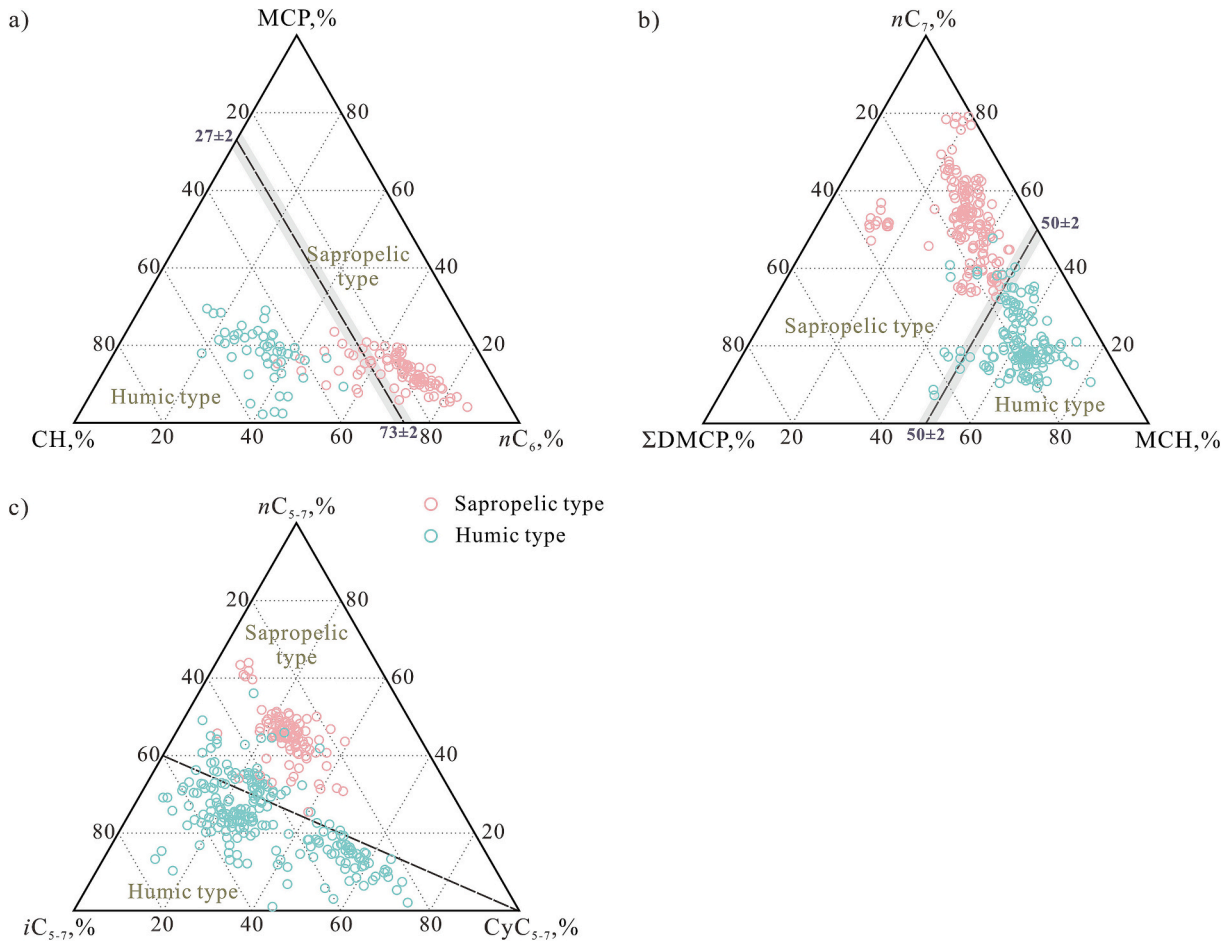

Fig. 7. Ternary diagrams showing the relative normalized abundance of (a) MCP (MCP: methylcyclopentane), CH (CH: cyclohexane), and nC_6 (nC_6: *n*-hexane) (modified from Hu et al., 1990); (b) nC_7 (nC_7: *n*-heptane), ∑DMCP (DMCP: dimethylcyclopentane), and MCH (MCH: methylcyclohexane) (modified from Hu et al., 1990); (c) nC_{5-7}, iC_{5-7}, and CyC_{5-7} (modified from Dai, 1992). (For details of the data sources, see Fig. A.5).

kerogen cracking gas from oil cracking gas in the high-mature to over-mature stages (Fig. 6). The $\ln(C_2/C_3)$ vs. $\ln(C_1/C_2)$ crossplot, combined with an analysis of sample data, effectively distinguishes oil cracking gas from kerogen cracking gas and serves as a reliable indicator of the sample's thermal maturation stage (Fig. 6).

5. Depositional environment and organic matter source

5.1. Chemical Compositions

In recent decades, LH parameters have come to be widely employed in petroleum geology. They are used to characterize the organic matter sources and depositional environments of their corresponding source rocks, based on stability differences in their molecular configurations and their distinct sources (Hu et al., 2007; Hu et al., 1990; Odden et al.,

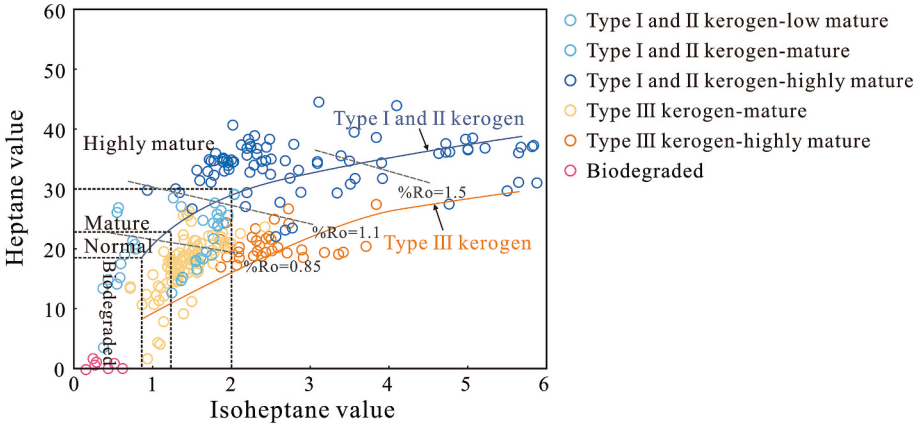

Fig. 8. Diagrams of heptane value versus isoheptane value (modified from Thompson, 1983). (For details of the data sources, see Fig. A.6).

1998; Mango, 1997; Dai, 1992).

Early studies demonstrated that the C_5-C_7 compound series correspond to various parent material sources. For instance, MCH primarily originates from sugars, cellulose, and lignin in higher plants, while DMCP is predominantly derived from terpenoids and steroids in aquatic organisms. *N*-heptane (nC_7) is chiefly sourced from bacteria and algae (Clayton et al., 1991; Dai et al., 2014). Additionally, the LH composition of sapropelic organic matter is distinguished by a high concentration of *n*-paraffins, whereas humic organic matter is enriched in isoparaffins and aromatics. Cycloalkanes are also a distinctive feature of terrigenous organic matter (Snowdon and Powell, 1982; Leythaeuser et al., 1979). Building on these findings, a series of ternary diagrams were developed to classify organic matter types based on the source characteristics of LHs. These include the MCP-CH-nC_6, nC_7-∑DMCP-MCP, and nC_{5-7}-iC_{5-7}-CyC_{5-7} ternary diagrams (Fig. 7). A review of LH data from oil and gas reservoirs across various global basins indicates that these diagrams generally provide reliable classification of organic matter types. However, samples located near boundary lines are often difficult to classify reliably (Fig. 7). Hu et al. (1990) proposed that in the MCP-CH-nC_6 and nC_7-∑DMCP-MCH ternary diagrams, the contents of CH and MCH in humic organic matter typically exceed 27 ± 2 % and 50 ± 2 %, respectively (Fig. 7a and b). Analysis of the collected data points indicates that only a few were misclassified near the critical boundary, which may be attributed to the varying contributions of different types of organic matter (Huang et al., 2022). Secondary alteration and hydrocarbon migration may, however, significantly affect light hydrocarbon parameters. Certain sapropelic-type oil samples from the Shunbei area are plotted within the humic-type domain (Fig. A.5a; Qiao et al., 2024b). This shift is primarily attributed to the preferential loss of *n*-alkanes during intense evaporative fractionation (Losh et al., 2002). Conversely, some humic-type samples, including gas from the Ordos Basin and retrograde condensates from the Junggar Basin, appear within the sapropelic-type area (Fig. A.5b; Sun et al., 2016; Ni et al., 2024). Previous studies suggest that gas migration can enrich samples in *n*-alkanes (Sun et al., 2016; Ni et al., 2024). In contrast, the nC_{5-7}-iC_{5-7}-CyC_{5-7} ternary diagram shows poorer differentiation (Fig. 7c). This chart is empirical, derived from a limited sample set, and lacks a solid theoretical foundation (Dai, 1992). Therefore, classification results near diagram boundaries should be interpreted with caution when using ternary classification diagrams.

Thompson (1983) showed that the H values of samples from sapropelic organic matter were significantly higher than those from humic samples under similar maturity conditions. Therefore, both the H and I values can be used for classifying organic matter types (Fig. 8). Other parameters, including Bz content, Tol content, the methylcyclohexane index (MCH/(MCH + nC_7 + ∑DMCP)), and the cyclohexane index (CH/(CH + MCP + nC_6)), can also be used for this purpose (Zhang and Li, 2001; Hu et al., 1990).

During geological evolution, specific LH compound types typically predominate under different depositional conditions (Mango, 1994). For instance, CH is predominant in terrigenous oils derived from higher plants, indicating a six-ring preference (6RP). In contrast, marine oils exhibit a five-ring preference (5RP), while lacustrine oils show a three-ring preference (3RP) (ten Haven, 1996; Mango, 1987). The LHs parameter K2 (K2 = P3 / (P2 + N2), N2 = (1, 1- + 1, c3- + 1, t3-) DMCP, P2 = (2- + 3-) MH), proposed by Mango (1990), has been shown to effectively distinguish marine from terrigenous oils. Typically, the K2 value of marine oil exceeds that of terrigenous oil (Zhu and Zhang, 1999).

Certain LHs compounds, such as diamondoids and alkylbenzenes, originate directly from source rocks (Dahl et al., 1999). Under acidic conditions, diamondoids are synthesized from various types of organic matter through a positive carbon ion medium. Low molecular weight alkylbenzenes form through cleavage of C—C bonds between isorenieratenes and kerogens (Koopmans et al., 1996; Hartgers et al., 1994). Schulz et al. (2001) proposed the DMDI-1 parameter (DMDI-1 =

Table 2
Light hydrocarbon parameters or diagram for identifying deposition environment and organic matter sources.

Parameter(s)/diagram(s)	Relation	Source(s)
H (H=(nC_7 × 100 %)/(CH + 2MH + 2, 3DMP + 1, 1DMCP + 3MH + 1c3-DMCP +1 t3-DMCP +1 t2-DMCP + nC_7 + MCH)); I (I = (2 + 3)-MH × 100 %/(1c3 + 1 t3 + 1 t2)-DMCP)	Type I and II kerogen > Type III kerogen (similar maturity)	Thompson, 1983
C_7 (ΣDMCP–nC_7–MCH)	triangle diagram (Fig. 7b)	Hu et al., 1990
C_{5-7} (iC_{5-7}–nC_{5-7}–CyC_{5-7})	triangle diagram (Fig. 7c)	Hu et al., 1990
I_{MCH} = MCH × 100 %/(MCH + nC_7 + 1c3-DMCP +1 t3-DMCP +1 t2-DMCP +1, 1DMCP + ECP)	<50 ± 2 %: Type I and II kerogen (Sapropelic); >50 ± 2 %: Type III kerogen (Humic)	Hu et al., 1990
I_{CH} = CH × 100 %/(CH + nC_6 + MCP)	<27 ± 2 %: Type I and II kerogen (Sapropelic); >27 ± 2 %: Type III kerogen (Humic)	Hu et al., 1990
C_6 (CH–MCP–nC_6)	triangle diagram (Fig. 7a)	Hu et al., 1990
K2 (K2 = P3/(P2 + N2))	marine oils: 0.20 < k2 < 0.23; terrigenous oils: 0.29 < k2 < 0.36	Mango, 1990; Zhu and Zhang, 1999
3RP (isoparaffins), 5RP (cyclopentanes), 6RP (cyclohexanes)	3RP: lacustrine oils; 5RP: marine oils; 6RP: terrigenous oils	Mango, 1994; Ten Haven, 1996
The contents of Bz, Tol and cycloalkanes	the contents of Bz, Tol and MCH in the samples of humic type sample are high	Zhang and Li, 2001
DMDI-1 (DMDI-1 = 3, 4DMD/(3, 4DMD + 4, 9DMD) × 100 %); EAI (EAI = 2EA/(2EA + 1EA) × 100 %)	DMDI-1 < 75 % and EAI < 80 %: Type II (marine); DMDI-1 > 75 % and EAI > 80 %: Type III (terrestrial)	Schulz et al., 2001
MT1 (MT1 = 3-ethyl-2-methylheptane/3methylnonane); MT2 (MT2 = 1, 1, 2, 3-tetramethylcyclohexane/propylcyclohexane)	MT1 and MT2 > 0.5: anoxic conditions MT1 and MT2 < 0.5: oxic conditionss	Wang et al., 2014
MTR (MTR = 2-methyl-3-ethylheptane/2, 6-dimethyloctane)	>0.4: reducing conditions (marine oils); <0.3: oxic/sub-oxic conditions (terrigenous oils)	Cheng et al., 2015a
TeMBr (TeMBr = 1, 2, 3, 5−/1, 2, 3, 4-tetramethylbenzene)	>1.5: oxic/dysoxic depositional environment; <1.0: anoxia depositional environment	Cheng et al., 2015b
C_8R ratio (C_8R = (1 t4- + 1c3- + 1, 1-) DMCH/(ctc, 1, 2, 4-TMCP + ctc, 1, 2, 3-TMCP))	>5: terrigenous plant input under oxic to suboxic conditions; <5: anoxic, carbonate environment	Chang et al., 2017
DMEBR-1 (DMEBR-1 = (1, 3-DM-2-EB + 1, 2-DM-2-EB)/1, 2, 3, 4-TeMB); DMEBR-2 (DMEBR-2 = (1, 4-DM-2-EB + 1, 3-DM-4-EB + 1, 2-DM-4-EB + 1, 3-DM-2-EB + 1, 2-DM-3-EB)/(1, 2, 4, 5-TeMB +1, 2, 3, 5-TeMB +1, 2, 3, 4-TeMB)); 1-MiPBR (1-MiPBR = (1-M-2-iPB + 1-M-3-iPB + 1-M-4-iPB)/(1, 2, 3, 5-TeMB +1, 2, 3, 4-TeMB))	DMEBR-1 > 0.8 and DMEBR-2 > 0.9 and 1-MiPBR >0.6: oxic-suboxic and freshwater and terrigenous (OM); DMEBR-1 < 0.8 and DMEBR-2 < 0.9 and 1-MiPBR<0.6: anoxix, reducing, and brackish-saline water and algal organic matter (OM)	Zhan et al., 2023

H: heptane values; I: isoheptane values; nC_5: *n*-pentane; nC_6: *n*-hexane; nC_7: *n*-heptane; CH: cyclohexane; MH: methylhexane; DMP: dimethylpentane; DMCP: dimethylcyclopentane; MCH: methylcyclohexane; MCP: methylcyclopentane; DMCH: dimethylcyclohexane; DMD: dimethyldiamantane; TMCP: trimethylcyclopentane; EA: Ethyladamantane; P2 = 2MH + 3MH; P3 = 3-ethylpentane +3,

3DMP + 2, 3DMP + 2, 4DMP + 2, 2DMP; N2 = 1, 1DMCP + 1, 3DMCP (cis + trans); RP: ring preference; Tol: toluene; Bz: benzene; DMDI-1: Dimethyl diamantane index 1; EAI: Ethyl adamantane index; MTR: monoterpane ratio; DMEBR: dimethylethylbenzene ratio, MiPBR: methylisopropylbenzene ratio; TeMB: tetramethylbenzene, M: methyl; DM: dimethyl; iPB: isopropylbenzene; EB: ethylbenzene; ECP: ethylcyclopentane.

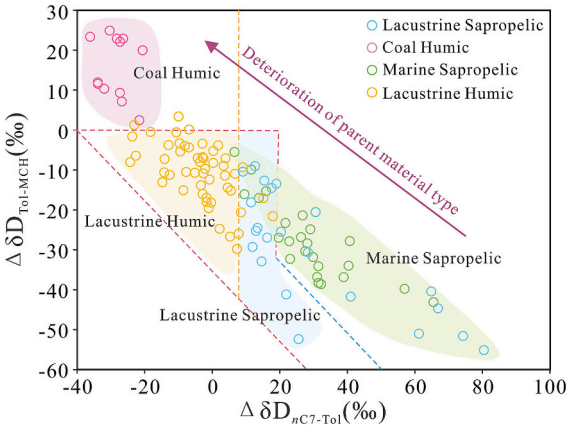

Fig. 9. Diagrams of $\Delta\delta D_{Tol-MCH}$ (Tol: toluene; MCH: methylcyclohexane) versus $\Delta\delta D_{nC7-Tol}$ (nC_7: *n*-heptane) (modified from Deng et al., 2023). (For details of the data sources, see Fig. A.7).

3, 4DMD/(3, 4 + 4, 9) DMD × 100 %) and the EAI parameter (EAI = 2EA/(2EA + 1EA) × 100 %) to differentiate marine from terrestrial depositional environments. Cheng et al. (2015b) proposed the TeMBr ratio (TeMBr = 1, 2, 3, 5−/1, 2, 3, 4-Tetramethylbenzene (TEMB)) for distinguishing depositional environments using the GC × GC-TOFMS method. The principle is that 1, 2, 3, 5-TEMB is abundant in oil from source rocks deposited under oxic conditions, whereas its content is very low under reductive conditions. However, this parameter may decrease significantly during the high thermal evolution stage due to variations in the formation rates or thermal stability of the compound (Zhan et al., 2023).

With advances in technology, more geochemical indicators have emerged for high-carbon-number LHs. Cheng et al. (2015a) analyzed LHs in 49 oil samples from the Tarim Basin using GC × GC-TOFMS. They found 2-methyl-3-ethylheptane (2-M-3-EH) and 2, 6-dimethyloctane (2, 6DMO) to be the predominant compounds and proposed the monoterpene ratio (MTR), which is defined as the ratio of 2-M-3-EH to 2, 6DMO. This ratio correlates well with classical geochemical parameters, including the dibenzothiophene/phenanthrene (DBT/P) and pristane/phytane (Pr/Ph) ratios, which supports its reliability. An MTR greater than 0.4 indicates a reducing environment, while an MTR below 0.3 suggests an oxidizing environment (Cheng et al., 2015a). Wang et al. (2014) further proposed 3-ethyl-2-methylheptane/3-methylnonane (MT1) and 1, 1, 2, 3-tetramethylcyclohexane/propylcyclohexane (MT2), which effectively differentiate depositional environments. Chang et al. (2017) used this instrument to analyze C_8 LHs in 23 oil samples and proposed a new depositional environment index—C_8 LHs ratio (C_8R). Marine oils typically have low C_8R values, while terrestrial oils have high C_8R values. Table 2 presents the relevant parameters and classification criteria for identifying organic matter sources and depositional environments, including new parameters as well as the parameters previously mentioned.

5.2. *Stable isotopic compositions*

The carbon isotopes of LHs ($\delta^{13}C_{LHs}$) typically exhibit strong parental genetic characteristics. $\delta^{13}C_{LHs}$ formed from different types of source rocks can vary significantly (Halpern, 1995; Wever, 2000). Specifically, those from humic kerogen are notably heavier than those from sapropelic kerogen (Huang et al., 2022). Previous research has shown that hydrogen undergoes a greater degree of isotopic fractionation compared to carbon when C—H bonds in hydrocarbons break (Cheng et al., 2018). Consequently, hydrogen isotopes (δD) in LHs are more reliable than $\delta^{13}C$ for identifying samples near the critical boundary.

Deng et al. (2023) used the δD of LHs to distinguish between coal-formed oil (humic type), lacustrine oil (humic type), lacustrine oil (sapropelic type), and marine oil in the Tarim Basin. The results indicate that the δD_{MCH}–δD_{Tol}–δD_{nC7} values exhibit strong, weak, and inverse V-type distributions in marine, lacustrine, and coal oils, respectively (Deng et al., 2023). Deng et al. (2023) developed the $\Delta\delta D_{Tol-MCH}$ vs. $\Delta\delta D_{nC7-Tol}$ intersection plot to differentiate organic matter sources and depositional

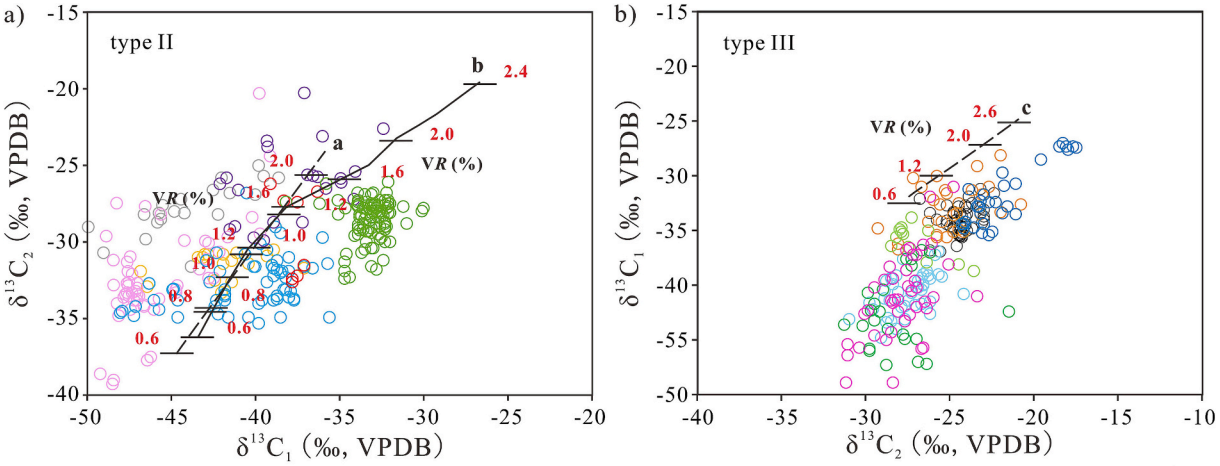

type II: Langgu Sag, Jizhong Depression, Bohai Bay Basin[1] Tazhong area, Tarim Basin central Sichuan Basin[2] Shunbei oilfield, Tarim Basin Shunnan area, Tarim Basin deep clastic reservoirs, Junggar Basin[3] mid−eastern Ordos Basin[4]

type III: Taibei sag, Tu−Ha Basin[5] Upper Paleozoic, Ordos Basin[5] Huanghua Depression, Bohai Bay Basin[5] Santanghu Basin[5] Kuche Depression, Tarim Basin[5] Northeastern part of the Sichuan Basin[5] Liaohe depression, Bohai Gulf Basin[5]

Fig. 10. Diagrams of (a) $\delta^{13}C_1$ versus $\delta^{13}C_2$ (a from Faber, 1987; b from Berner and Faber, 1996); (b) $\delta^{13}C_2$ versus $\delta^{13}C_1$ (c from Berner and Faber, 1996). Data 1 from Chen et al., 2022; 2 from Fu, 2023; 3 from Kang et al., 2021; 4 from Yang et al., 2022; 5 from Liu, 2015; and 6 from Pei et al., 2023.

environments based on these variations (Fig. 9). The $\Delta\delta D_{nC7\text{-}Tol}$ values for coal-formed (humic type), lacustrine, and marine oils range from less than −20 ‰, between −20 ‰ and 20 ‰, and greater than 6 ‰, respectively. The $\Delta\delta D_{Tol\text{-}MCH}$ values for coal, lacustrine, and marine oils range from >0 ‰, −30 ‰ to 0 ‰, and < −5 ‰, respectively (Fig. 9).

6. Maturity

6.1. Nature gas maturity evaluation

Identifying the source and origin of natural gas in the field has always been a challenge. The conventional diagrams used for identifying the genetics of natural gas frequently fail to provide accurate results. In such cases, the thermal evolution of natural gas can provide a crucial reference for determining its sources and genesis.

Research on the maturation of natural gas dates back to the 1970s. Building on the characteristic that the $\delta^{13}C$ of natural gas becomes progressively heavier with thermal evolution, several empirical formulas and diagrams have been developed for identifying natural gas maturity (Chen et al., 2021; Stahl, 1977; Dai et al., 1987; Shen et al., 1987; Schoell, 1980; Stahl and Carey, 1975; Faber, 1987).

Natural gas maturity identification diagrams for type III and type II kerogen were developed in early studies based on pyrolysis experiment models and carbon isotope data (Faber, 1987; Berner et al., 1995). These diagrams assessed natural gas maturity by using the $\delta^{13}C_1$ and $\delta^{13}C_2$ variations of natural gas produced from kerogen during thermal evolution (Fig. 10). However, upon analyzing the collected data, it was found that the maturity identification results were suboptimal. Early studies indicated that Sinian-Cambrian natural gas in the Sichuan Basin primarily originates from oil cracking during the high- to over-mature stage (Ro > 2.0 %) (Fig. 6; Xie et al., 2021). However, the maturity distribution obtained from the diagram ranged from 1.0 % to 1.6 % (Fig. 10a), notably lower than the actual maturity of the natural gas. Similarly, the maturity estimation for humic-type gas yielded low results (Fig. 10b). These discrepancies may be due to the fact that $\delta^{13}C_2$ are less sensitive to maturity and primarily reflect organic matter type (Stahl, 1974). Additionally, isotopic reversals occur due to the influence of reaction rates and kinetic isotope effects (Fuex, 1977; Liu et al., 2018a; Coleman et al., 1981). Ethane, enriched in ^{12}C, is formed as a result of the thermal cracking of wet-gas components and potentially through isotope fractionation initiated by free radical decomposition or polymerization reactions at higher maturity (Cesar et al., 2020). The inversion of carbon isotopes in alkanes (where the carbon isotope value of heavier hydrocarbons becomes lighter) during the high-mature and over-mature stages renders the $\delta^{13}C_2$ values unsuitable for maturity determination. This phenomenon also occurs in shale and coalbed gas, as exemplified by over-mature shale gas in the Sichuan Basin and over-mature coalbed gas in the Ordos Basin (Fig. 10; Dai et al., 2016). For the reasons outlined above, an increasing number of studies have focused on the empirical relationship between $\delta^{13}C_1$ and the source rock's vitrinite reflectance (Ro; Xu, 1994; Dai et al., 1987; Stahl, 1977; Faber, 1987; Shen et al., 1987; Schoell, 1980). Sapropelic-type gas and humic-type gas are treated separately in the conversion of equivalent vitrinite reflectance (Rc) (Fig. 11). Comparative analysis reveals that the empirical formulas linking $\delta^{13}C_1$ and the Rc established by different researchers vary significantly (Fig. 11). However, earlier studies were primarily based on limited data and showed notable regional limitations. As a result, there are considerable discrepancies in the calculated values derived from different empirical formulas (Tables 3 and 4). Chen et al. (2021) reviewed and compared the existing empirical formulas for $\delta^{13}C_1$ and Rc and reconstructed the formulae for both sapropelic-type gases (Fig. 11a) and humic-type gases (Fig. 11b). Eq. (1) is the formula for calculating the maturity of sapropelic-type gas. Eq. (2) is the formula for calculating the maturity of humic-type gas.

$$lgRc = 0.04 \times \delta^{13}C_1 + 1.7 \quad (1)$$

$$lgRc = 0.04 \times \delta^{13}C_1 + 1.5 \quad (2)$$

The calculation results show that, for sapropelic-type gas, Chen et al. (2021)'s empirical formula yields a maturity distribution range of 1.67 %–2.83 % for oil cracking gas in Sichuan and 0.38 %–1.01 % for kerogen cracking gas in the Arkoma Basin (Table 3). These results generally agree with the thermal maturity of the corresponding source rocks and correspond to the identification outcomes from the $\ln(C_1/C_2)$ vs. $\ln(C_2/C_3)$ crossplot (Fig. 6). However, the maturity distribution calculated by the empirical formula for the mixture of oil cracking gas and kerogen cracking gas in the Shunbei area of the Tarim Basin ranges from 0.54 % to 1.37 % (Table 3). This result is inconsistent with the actual geological conditions (Qiao et al., 2024a, 2025b). The Tarim Basin underwent rapid deep burial during the Himalayan orogeny (Qiu et al., 2022), which caused a dramatic increase in confining pressure, restraining the thermal cracking of oil in these ultra-deep reservoirs. Moreover, the Tarim Basin exhibits a generally low geothermal gradient, and the Cambrian and Ordovician source rocks in the northern and central

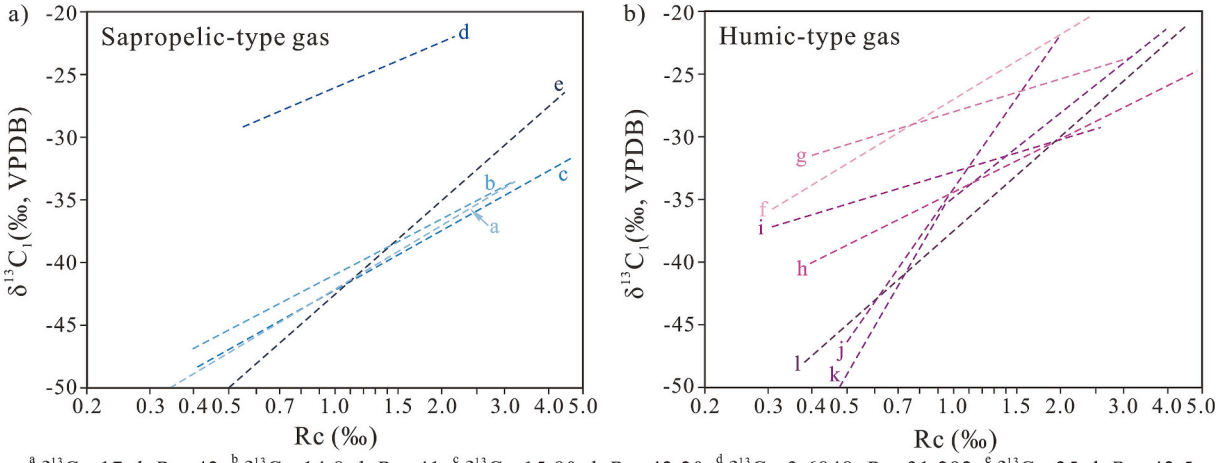

[a] $\delta^{13}C_1$=17×lgRc−42; [b] $\delta^{13}C_1$=14.8×lgRc−41; [c] $\delta^{13}C_1$≈15.80×lgRc−42.20; [d] $\delta^{13}C_1$=3.6848×Rc−31.292; [e] $\delta^{13}C_1$=25×lgRc−42.5; [f] $\delta^{13}C_1$=14×lgRc−28; [g] $\delta^{13}C_1$=8.6×lgRc−28; [h] $\delta^{13}C_1$≈14.12×lgRc−34.39; [i] $\delta^{13}C_1$=8.6411×lgRc−32.8; [j] $\delta^{13}C_1$=40.49×lgRc−34; [k] $\delta^{13}C_1$=48.77×lgRc−34.1 (Ro≤0.9%); $\delta^{13}C_1$=22.42×lgRc−34.8 (Ro>0.9%); [l] $\delta^{13}C_1$=25×lgRc−37.5

Fig. 11. Diagrams of (a) Rc (‰) versus $\delta^{13}C_1$; (b) Rc (‰) versus $\delta^{13}C_1$. a and f from Stahl, 1977; b and g from Schoell, 1980; c and h from Dai et al., 1987; d from Berner et al., 1995; e and l from Chen et al., 2021; i from Shen et al., 1987; j from Xu, 1994; and k from Liu and Xu, 1999.

Table 3
Maturity of oil-type gas calculated using different empirical equations.

Basin	Data set	$\delta^{13}C_1$	[a]Rc, %	[b]Rc, %	[c]Rc, %	[d]Rc, %	[e]Rc, %	Source
Arkoma Basin	Woodford Shale	−53.0 ~ −42.4 −48.7 (15)	0.22–0.95 0.48	0.15–1.19 0.40	0.21–0.98 0.47	/	0.38–1.01 0.61	Liu et al., 2019
Tarim Basin	Shunbei oilfield	−49.2 ~ −39.1 −45.1 (56)	0.38–1.48 0.63	0.28–2.71 2.55	0.36–1.57 0.63	/	0.54–1.37 0.75	this paper
Junggar Basin	Mahu Sag	−54.4 ~ −37.1 −45.5 (24)	0.19–1.94 0.79	0.12–1.83 0.67	0.17–2.10 0.81	/	0.33–1.64 0.85	Kang et al., 2021
Ordos Basin	the mid-eastern Ordos Basin	−42.1 ~ −32.4 −36.5 (51)	0.99–3.67 2.22	0.81–3.81 2.11	1.01–4.17 2.43	/	1.04–2.54 1.78	Yang et al., 2022
Sichuan Basin	Northwestern part	−36.9 ~ −31.2 −34.3 (39)	2.00–4.32 2.88	1.89–4.59 2.90	2.16–4.97 3.21	/~0.02 /	1.67–2.83 2.14	Pei et al., 2023

a: $\delta^{13}C_1 = 17 \times \lg(Rc) - 42$ (Stahl, 1977); b: $\delta^{13}C_1 = 14.8 \times \lg(Rc) - 41$ (Schoell, 1980); c: $\delta^{13}C_1 \approx 15.80 \times \lg(Rc) - 42.2$ (Dai et al., 1987); d: $\delta^{13}C_1 = 3.6848 \times Rc - 31.292$ (Berner et al., 1995); e: $\delta^{13}C_1 = 25 \times \lg(Rc) - 42.5$ (Chen et al., 2021).

Table 4
Maturity of coal-type gas calculated using different empirical equations.

Basin	Data set	$\delta^{13}C_1$	[f]Rc, %	[g]Rc, %	[h]Rc, %	[i]Rc, %	[j]Rc, %	[k]Rc, %	[l]Rc, %	Source
Qiongdongnan Basin	Y13, L25, LS13, L17, L18, S34, Y8	−46.8 ~ −35.0 −40.6 (44)	0.05–0.32 0.15	0.01–0.15 0.05	0.13–0.90 0.42	0.02–0.55 0.18	0.48–0.94 0.70	0.55–0.96 0.75	0.42–1.26 0.79	Liang et al., 2020
Turpan-Hami Basin	Taibei Sag	−44.8 ~ −36.9 −40.7 (44)	0.06–0.23 0.13	0.01–0.09 0.04	0.18–0.66 0.37	0.04–0.34 0.14	0.54–0.85 0.69	0.60–0.88 0.73	0.51–1.06 0.75	Pei et al., 2023
Ordos Basin	Upper Paleozoic	−36.7 ~ −28.1 −32.9 (34)	0.24–0.98 0.48	0.10–0.97 0.32	0.69–2.79 1.36	0.35–3.50 1.15	0.86–1.40 1.07	0.82–1.99 1.25	1.08–2.38 1.56	Pei et al., 2023
	Zhidan-Ganquan area	−32.1 ~ −27.6 −28.7 (5)	0.51–1.08 0.92	0.33–1.13 0.89	1.44–3.05 2.6	1.19–4.04 3.21	1.11–1.44 1.35	1.31–2.10 1.89	1.64–2.50 2.27	Chen et al., 2020
Tarim Basin	Kuche Depression	−35.4 ~ −27.0 −31.7 (31)	0.30–1.18 0.61	0.14–1.30 0.5	0.85–3.34 1.74	0.50–4.70 1.81	0.92–1.49 1.16	0.94–2.23 1.44	1.21–2.63 1.77	Pei et al., 2023
Junggar Basin	Southern	−37.0 ~ −25.3 −31.6 (22)	0.23–1.56 0.66	0.09–2.06 0.59	0.66–4.40 1.86	0.33–7.38 2.12	0.84–1.64 1.17	0.80–2.65 1.49	1.05–3.08 1.82	Yu et al., 2024

f: $\delta^{13}C_1 = 14 \times \lg(Rc) - 28$ (Stahl, 1977); g: $\delta^{13}C_1 = 8.6 \times \lg(Rc) - 28$ (Schoell, 1980); h: $\delta^{13}C_1 \approx 14.12 \times \lg(Rc) - 34.39$ (Dai et al., 1987); i: $\delta^{13}C_1 = 8.6411 \times \lg(Rc) - 32.8$ (Shen et al., 1987); j: $\delta^{13}C_1 = 40.49 \times \lg(Rc) - 34$ (Xu, 1994); k: $\delta^{13}C_1 = 48.77 \times \lg(Rc) - 34.1$ ($Ro \leq 0.9$ %); $\delta^{13}C_1 = 22.42 \times \lg(Rc) - 34.8$ ($Ro > 0.9$ %) (Liu and Xu, 1999); l: $\delta^{13}C_1 = 25 \times \lg(Rc) - 37.5$ (Chen et al., 2021).

uplifts remain within the oil window (Jiang and Liu, 2025). This leads to the retention of a high proportion of sapropelic-type gas in the reservoir. The mixing of natural gas from various thermal evolution stages complicates the identification of its maturity. Early researchers proposed that natural gas maturity increased monotonically with $\delta^{13}C_1$ values (Fig. 11). However, simulation experiments reveal that the $\delta^{13}C_1$ values do not change monotonically during thermal evolution. In the early thermal evolution stages, the $\delta^{13}C_1$ values show a trend of initially decreasing and then increasing (Gao et al., 2018; Peng et al., 2020). This occurs because functional groups containing heteroatoms, such as oxygen (which is enriched in ^{12}C), are released first, causing a decline in the $\delta^{13}C_1$ values (He et al., 2018). Once these heteroatom-containing functional groups are depleted, the $\delta^{13}C_1$ values increase due to thermodynamic isotope fractionation. Consequently, the formula for calculating the maturity of the $\delta^{13}C_1$ values is unsuitable for precisely determining the maturity of natural gas in the early thermal evolution stages.

Humic-type gas has a simpler composition than sapropelic-type gas. Although a limited amount of oil forms during the thermal evolution of type III kerogen, gas is still the dominant product (Prinzhofer et al., 2000; Schoell, 1980). The data collected in this study show that the empirical formula for vitrinite reflectance and humic-type gas proposed by Chen et al. (2021) aligns well with the thermal evolution of source rocks in the geological context (Table 4). However, the $\ln(C_2/C_3)$ vs. $\ln(C_1/C_2)$ diagram reveals a significantly lower maturity assessment for humic-type gas at the high- to over-mature stage (Fig. 6).

6.2. Oil maturity evaluation

The relative thermal stability of LHs with the same carbon numbers typically follows the order: cycloalkanes < isoparaffins < *n*-paraffins < aromatics (Thompson, 1979; Odden et al., 1998). Mango (1997) proposed using the ratio 2, 4−/2, 3DMP to estimate oil formation temperatures (maximum temperature during burial), with the formula: T (°C) = 15[Ln (2, 4−/2, 3-DMP)] + 140. Many studies subsequently developed LH maturity parameters based on the differences in the thermal stability of compounds with the same carbon numbers.

Thompson (1983) proposed that H and I values effectively distinguish oil maturity, and these parameters have been widely used in petroleum basins around the world (Fig. 8, Abrams and Thomas, 2020; Obermajer et al., 2002; Khairy et al., 2022; Zhang et al., 2024; Srinivasan et al., 2022). The H—I value intersection diagram divides the maturity range into four regions: biodegradation, normal oil, mature, and high mature (Fig. 8). However, the diagram serves only as a rough guide to an oil's maturity.

Schaefer et al. (1984) analyzed source rock samples from the Elmworth gas field, western Canada, and found that the cyclopentane/C_5 hydrocarbon ratio decreased with depth. Schaefer and Littke (1988) subsequently analyzed shale samples from the Lower Saxony Basin, northern Germany, and proposed two maturity parameters: the V index (C_7 paraffin/naphthene concentration ratio) and the J index (ratio of (2- + 3-) MH /(1c3-, + 1 t3-, + 1 t2-, + 1c2-) DMCP). Both parameters correlate strongly with Ro. The formulas for calculating equivalent vitrinite reflectance are %Rc = 1.8log(V) + 1.00 and %Rc = 1.1log(J) +

Table 5
Light hydrocarbon parameters or diagram for assessing maturity.

Parameter(s)/diagram(s)	Correlation	equivalent vitrinite reflectance (%Rc)	application scope, influence factor	Source(s)
Alkane/cycloalkane	Positive			Philippi, 1975
iC_5/nC_5	Increased between 50 and 90 °C, then decreased with increasing temperature		Ro < 0.8 %	Hunt et al., 1980b
H and I	Positive (Fig. 8)		biodegradation	Thompson, 1983
Relative cyclopentane content and the concentration ratio of the 1, 2-dimethylcyclopentane stereoisomers	Negative			Schaefer et al., 1984
Branched/straight chain alkanes	Negative			Hunt, 1984
B (B = Tol/nC_7), F (F = nC_7/MCH)	Positive (Fig. 12)			Thompson, 1987
2, 4DMP/2, 3DMP	Positive			Mango, 1987
V (V = C_7 paraffin/naphthene concentration ratio)	Positive	Rc=1.0 + 1.8logV		Schaefer and Littke, 1988
J (J = (2-MH + 3-MH)/(1c3- + 1 t3- + 1 t2- + 1c2-)DMCP concentration ratio)	Positive	Rc = 0.84 + 1.1logJ		Schaefer and Littke, 1988
R1 (R1 = 1 t2-DMCP/1c2-DMCP concentration ratio)	Negative			Schaefer and Littke, 1988
iC_4/nC_4	Positive		Ro < 0.8 %, biodegradation	Hou et al., 1989
MAI (MAI = 1MA/(1MA + 2MA) × 100 %)	Positive			Chen et al., 1996
MDI (MDI = 4MD/(1MD + 3MD + 4MD) × 100 %)	Positive	Rc = 0.0243MDI + 0.4389	Ro: 0.9–2.0 %	Chen et al., 1996; Li et al., 2000
T(°C) = 140 + 15 [Ln (2, 4DMP/2, 3DMP)]	Positive			Mango, 1997
EAI (EAI = 2EA/(2EA + 1EA) × 100 %)	Positive		Ro < 1.3 %, depositional environment	Schulz et al., 2001
DMDI-1 (DMDI-2 = 3, 4DMD/(4, 9DMD + 3, 3DMD))	Positive			Schulz et al., 2001
DMDI-2 (DMDI-2 = 4, 8DMD/(4, 9DMD + 4, 8DMD))	Positive			Schulz et al., 2001
TeMB-1 (TeMB-1 = 1, 2, 4, 5-TeMB/total TeMB); TeMB-2 (TeMB-2 = 1, 2, 3, 5-TeMB/total TeMB); TeMB-3 (TeMB-3 = (1, 2, 3, 5- + 1, 2, 4, 5-TeMB)/total TeMB)	Positive			Hill et al., 2004
TeMN-1 (TeMN-1 = 1, 3, 6, 7-TeMN/(1, 3, 6, 7-TeMN +1, 2, 5, 6-TeMN +1, 2, 3, 5-TeMN)); TeMN-2 (TeMN-1 = 1, 3, 6, 7-TeMN/(1, 3, 6, 7-TeMN +1, 2, 5, 7-TeMN)); TeMN-3 (TeMN-1 = 2, 3, 6, 7-TeMN/(2, 3, 6, 7-TeMN +1, 2, 3, 7-TeMN)); TeMN-4 (TeMN-1 = 1, 3, 6, 7-TeMN/ total TeMN))	Positive			Hill et al., 2004
DMEB-1 (DMEB-1 = 1, 4-DM2EB/(1, 4-DM2EB + 1, 3-DM2EB)); DMEB-2 (DMEB-2 = total DMEB/(total DMEB + total TeMB))	Positive	F		Hill et al., 2004
MiPB (MiPB = 1M4iP/(1M4iP + 1M3iP))	Positive			Hill et al., 2004
The concentrations of diamondoids	Positive			Wei et al., 2007
C_{3-4}/C_{0-2} alkylbenzenes	Negative		mixing	Cheng et al., 2015b
(m- + p-)/o-propyltoluene; (3, 5- + 3, 4-)/(2, 5- + 2, 4-ethylxylene)	Positive			Cheng et al., 2015b
O_1 value (O_1 = (2- + 3- + 4-)MC_7/ (t, 1, 4- + c, 1, 3- + 1, 1-)DMCH); O_2 value (O_2 = (nC_8 × 100)/(nC_8 + 2, 4DMH + 1cis, 2trans, 4cis-TMCP +1cis, 2trans, 3cis-TMCP +2, 3DMH + 2MC_7 + 4MC_7 + 3, 4DMH + 3MC_7 + 1cis, 3-DMCH +1trans, 4-DMCH +1, 1DMH+ 1-E, 3cis-MCP + 1trans, 2-DMCH))	Positive		biodegradation, water washing, evaporative fractionation, and high-temperature sulfate reduction	Chang et al., 2017
1, 2-DMEBR (1, 2-DMEBR = 1, 2-DM-4-EB/(1, 2-DM-4-EB + 1, 2-DM-3-EB))	Positive			Zhan et al., 2023
DM4EBR (DM4EBR = 1, 3-DM-4-EB/1, 2-DM-4-EB); TMBR (TMBR = 1, 2, 3TMB + (1, 2, 3TMB + 1, 2, 4TMB + 1, 3, 5TMB))	Negative			Zhan et al., 2023

iC_5: isopentane; nC_5: *n*-pentane; H: heptane values; I: isoheptane values; Tol: toluene; Bz: benzene; DMP: dimethylpentane; MH: methylhexane; DMCP: dimethylcyclopentane; iC_4: isobutane; nC_4: *n*-butane; MAI: methyl adamantane index; MDI: methyl diamantane index; T(°C): oil formation temperature (maximum temperature of burial); EAI: Ethyl adamantane index; EA: Ethyladamantane; DMDI: Dimethyl diamantane index 1; DMD: dimethyldiamantane; TeMB: Tetramethylbenzene; DMEB: dimethylethylbenzene; MiPB: methylisopropylbenzene; TeMN: Tetramethylnaphthalene; LHR: Light Hydrocarbon Ratio; O_1: isooctane; O_2: octane; MP: methylpentane; DMCH: dimethylcyclohexane; nC_8: *n*-octane; DMH: dimethylhexane; TMCP: trimethylcyclopentane; DMCH: dimethylcyclohexane; MCP: methylcyclopentane; DM: dimethyl; EB: ethylbenzene; TMBR: trimethylbenzene ratio; TMB: trimethylbenzene.

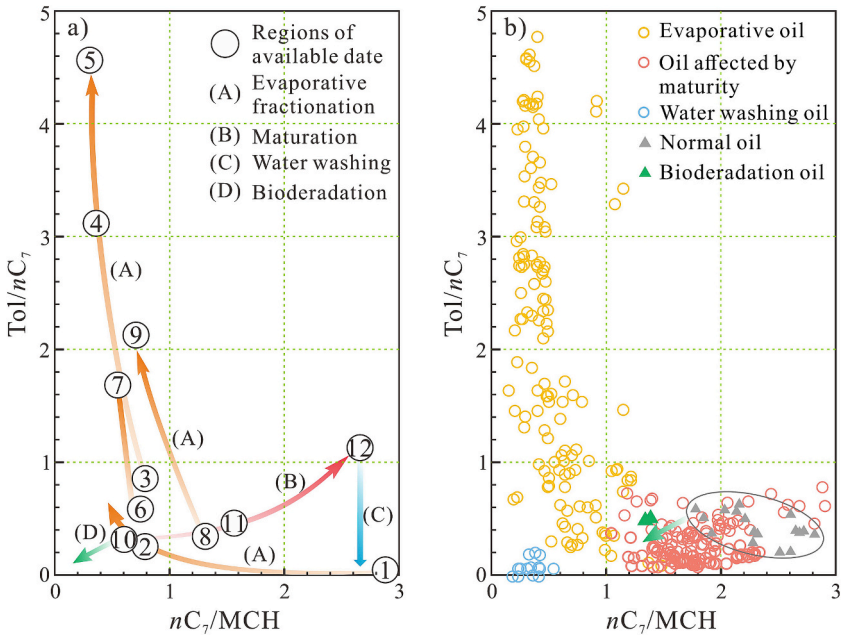

Fig. 12. Diagrams of nC_7/MCH (*n*-heptane/methylcyclohexane) versus Tol/nC_7 (toluene/*n*-heptane) (modified from Thompson, 1987). (For details of the data sources, see Fig. A.8).

0.84 (Schaefer and Littke, 1988). Whiticar and Snowdon (1999) noted that the result obtained using the V index differed significantly from that obtained using the J index. The applicability of the V and J indexes has, therefore, been questioned, limiting their use.

Numerous studies have subsequently proposed a succession of other maturity parameters, including the iC_4/nC_4 and iC_5/nC_5 ratios (Hou et al., 1989), the MiPB (methylisopropylbenzene ratio) (MiPB = (1M4iP/(1M4iP + 1M3iP), 1M4Ip: 1-Methyl-4-isopropylbenzene) (Hill et al., 2004), and C_{3-4}/C_{0-2} alkylbenzenes (Cheng et al., 2015b). However, most of these parameters primarily indicate the relative degree or range of maturity. The scope and the factors influencing the application of these parameters are detailed in Table 5.

Among the various maturity parameters of LHs, diamondoids are particularly notable for their unique molecular structures and thermal stability. Based on samples from the Qiongdongnan, Yinggehai, and Tarim basins in China, Chen et al. (1996) proposed that MAI (the methyladamantane index) and MDI (the methyldiamantane index) are effective indicators for assessing the maturity of source rocks. The formula for calculating %Rc based on MDI is as follows: %Rc = 0.4389 + 0.0243MDI (Chen et al., 1996). However, MAI is influenced by regional variations and evaporative fractionation, which limit its applicability (Qiao et al., 2024a; Qi et al., 2022; Schulz et al., 2001). MDI is more stable and has been widely applied in basins around the world with a maturity range of 0.9 % to 2.0 % (Li et al., 2000; Qiao and Chen, 2022; Qiao et al., 2024b). Other studies have also proposed other maturity parameters, including EAI (the Ethyl adamantane index, EAI = 2−/(2- + 1-) EA), DMDI-1 (the Dimethyl diamantane index 1, DMDI-1 = 3, 4−/(3, 4- + 4, 9-) DMD), and DMDI-2 (the Dimethyl diamantane index 2, DMDI-2 = 4, 8−/(4, 8- + 4, 9-) DMD) (Schulz et al., 2001). However, these parameters also have significant limitations, being confined to specific regions and being less widely applicable than MDI.

7. Secondary alteration

LHs are a key component of petroleum, making up large proportions of the compositions of highly mature oils (Hunt et al., 1980; Hunt, 1984). Highly mature oil can be influenced by various complex secondary alteration processes throughout their prolonged geological evolution, so assessing the impact of secondary alteration on LHs is crucial for further evaluating the accuracy of LH parameters.

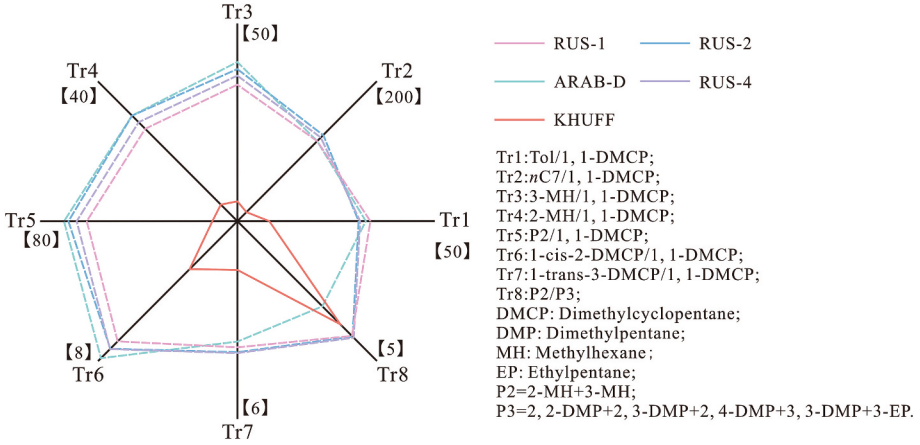

Fig. 13. C_7 oil transformation star diagram (modified from Halpern, 1995). (Data from Halpern, 1995).

7.1. Evaporative fractionation

Evaporative fractionation refers to the process by which natural gas dissolves oil in a reservoir, extracting low molecular weight hydrocarbons and separating them during natural gas charging (Qiao et al., 2024a; Thompson, 1987, 2010; Losh et al., 2002). Thompson (1987) observed in simulation experiments that oil becomes abnormally enriched in cycloalkanes and aromatics following evaporative fractionation. Subsequently, it was proposed that aromaticity (B, Tol/nC_7) and paraffinicity (F, nC_7/MCH) could effectively indicate whether oil had undergone evaporative fractionation (Fig. 12a; Thompson, 1987). Analysis of aggregated data reveals that B—F diagrams are widely used in petroleum fields (Fig. 12b).

Moldowan et al. (2015) found that the ratio of (1- + 2-) MA to (3- + 4-) MD in normal oil from the same source remains constant. However, during evaporative fractionation, natural gas removes a significant portion of (1- + 2-) MA, leaving a higher proportion of (3- + 4-) MD. As a result, the (1- + 2-) MA/(3- + 4-) MD ratio increases in newly formed light oils and decreases in residual oils (Qiao et al., 2024a, 2024b; Wang et al., 2023; Moldowan et al., 2015). This suggests that this ratio is an effective indicator of evaporative fractionation, enabling the differentiation of newly generated light oil reservoirs from residual oil reservoirs.

Previous studies have shown that dry gas charging typically leads to pronounced evaporative fractionation effects, reflected in notable changes in Tol/nC_7 ratios (Zhu et al., 2021b; Qiao et al., 2024c). In contrast, evaporative fractionation associated with wet gas charging tends to produce less pronounced variations in Tol/nC_7 ratios (Zhu et al., 2019; Qiao et al., 2024a). Moreover, (1- + 2- MA/ (3- + 4-) MD is not a reliable indicator of evaporative fractionation in the presence of thermochemical sulfate reduction (TSR) (Cai et al., 2016).

Table 6
Light hydrocarbon parameters or diagram for identifying secondary alteration processes.

Secondary alteration processes type	Parameter(s)/diagram (s)	Correlation	Source(s)
Biodegradation	H and I (Fig. 8)	H < 18, I < 0.8	Thompson, 1983
	B and F (Fig. 12)	Negative	Thompson, 1987
	Tr1 (Tr1 = Tol/1, 1DMCP); Tr2 (Tr2 = nC_7/1, 1DMCP); Tr3 (Tr3 = 3MH/1, 1DMCP); Tr4 (Tr4 = 2MH/1, 1DMCP); Tr5 (Tr5 = P2/1, 1DMCP); Tr6 (Tr6 = 1c2-DMCP/1, 1DMCP); Tr7 (Tr7 = 1 t3-DMCP/1, 1DMCP)	Negative (Fig. 13)	Halpern, 1995
	MA/A	Positive	Grice et al., 2000
	MDIA/DIA	Obvious change in the ratio only occurs at extreme levels of biodegradation (level 8)	Grice et al., 2000
	3MP/nC_6, iC_5/nC_5	Positive	George et al., 2002
	C_2/(C_2 + C_3) alkylbenzenes	Negative	George et al., 2002
	1, 2, 3-trimethylbenzene/Σtrimethylbenzenes	Positive	George et al., 2002
	2/3MH, 2/3MP (Fig. 14)	Negative	George et al., 2002
Evaporative fractionation	B and F	Fig. 12	Thompson, 1987
Water washing	Tr1	Positive	Halpern, 1995
Migration direction	Tol/MCH, Bz/3MP	Negative	Obermajer et al., 2000
	Bz/nC_6, Tol/nC_7, Bz/CH	Negative (as a free gas phase); Positive (as water-dissolving phase)	Yu et al., 2014; Wu et al., 2024a

H: heptane values; I: isoheptane values; Tol: toluene; DMCP: dimethylcyclopentane; MH: methylhexane; P2 = 2MH + 3MH; A: adamantane; MA: methyladamantane; MDIA: methyldiamantane; DIA: diamantane; MP: methylpentane; iC_5: isopentane; nC_5: *n*-pentane; nC_6: *n*-hexane; nC_7: *n*-heptane; MP: methylpentane; MCH: methylcyclohexane; Bz: benzene; CH: cyclohexane.

7.2. Water washing

Water washing is the process by which a significant proportion of water-soluble components in oil are lost under the influence of formation water, leading to changes in the oil's properties (Thompson, 1987; Halpern, 1995; Lafargue and Le Thiez, 1996). Thompson (1987) observed that, as washing intensifies, B decreases, as demonstrated by both simulation experiments and sample studies (Fig. 12a). Halpern (1995) suggested that Tr1 (Tol/1, 1DMCP) could indicate whether oil had undergone water washing, based on the differences in solubility between Tol and 1, 1DMCP in water (Fig. 13). However, water washing is frequently associated with biodegradation, particularly in shallow reservoirs (Halpern, 1995; Lafargue and Le Thiez, 1996). Both B and Tr1 can also be influenced by biodegradation (Thompson, 1987; Halpern, 1995), so it is essential when using these parameters to determine whether the oil has been washed or has undergone biodegradation.

7.3. Biodegradation

In shallow reservoirs (<88 °C), bacterial activity under anaerobic conditions typically results in oil biodegradation (Rice and Claypool, 1981; Stetter et al., 1993). Generally, the biodegradation resistance of LHs follows the order: cycloalkanes > aromatics > isoparaffins > *n*-paraffins (Wenger and Isaksen, 2002). The B—F diagrams developed by Thompson (1987) can also be used to identify biodegradation (Fig. 12a). However, the data collected in this study indicate that this trend represents a relative change (Fig. 12b). The diagram should be compared to normal oil to identify biodegradation. Additionally, the biodegradation resistance of LHs is influenced by the position and number of substituents (George et al., 2002). Halpern (1995) selected 1, 1DMCP, the most biodegradation-resistant among C_7 LHs, as a reference compound and proposed parameters from Tr2 to Tr7 for assessing biodegradation (Fig. 13 and Table 6).

George et al. (2002) observed that 2-methylalkanes are more

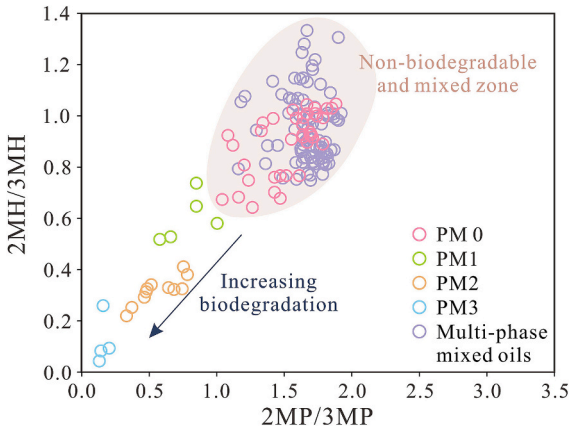

Fig. 14. Diagrams of 2MP/3MP (MP: methylpentane) versus 2MH/3MH (MH: methylhexane) (modified from George et al., 2002). (For details of the data sources, see Fig. A.9).

susceptible to bacterial degradation than 3-methylalkanes. Based on this, the ratios of 2-MP/3-MP (2-methylpentane/3-methylpentane) and 2-MH/3-MH were proposed as indicators of biodegradation intensity. Early studies indicate that isoparaffins in LHs are fully degraded when biodegradation reaches approximately PM 3 (PM is the Peters and Moldowan's scale) (Peters et al., 1996). Analysis of the data in this study shows that, for oil with biodegradation levels between PM0 and PM3, the intersection plot of 2/3MP and 2/3MH effectively identifies biodegradation (Fig. 14). However, the diagram is ineffective for identifying oil with multiphase mixing (Fig. 14). For example, previous studies indicate that there have been two stages of oil charging in the Shunbei area of the Tarim Basin, and that the oil accumulated early has experienced biodegradation (Qiao et al., 2024a). However, the distribution of sample points overlaps significantly with that of non-biodegraded oil (Fig. 14). This may be the result of the higher maturity of the late-charged oil, which contains a greater abundance of LHs. Consequently, the biodegradation signal in early-formed oil is obscured by the later-charged oil.

For stable isotopes of LHs, the $\delta^{13}C_1$ in the secondary microbial gas formed by biodegradation becomes lighter, and the stable carbon isotopes of their heavy hydrocarbon components become heavier (Masterson et al., 2001). The LHs carbon isotopes in the residual oil after biodegradation also show a tendency to become heavier (George et al., 2002).

7.4. Thermal cracking

Mango (2000) concluded that at reservoir temperatures exceeding 150 °C, LHs are primarily generated through the thermal cracking of oil. This perspective offers valuable insights into the origins of LHs in ultra-deep, highly mature oils. So far, conventional LHs parameters have not been effectively utilized to evaluate the degree of oil cracking.

Diamondoids, with their unique cage structure, will not crack during oil-to-gas conversion (Dahl et al., 1999). Based on this property, Dahl et al. (1999) used the absolute concentration of 3-MD (3-methyldiamantane) and 4-MD to quantify the extent of oil-to-gas conversion (EOC) (EOC = [1–(Co/Cc)] × 100 %, where Co is the absolute concentration of 4-MD and 3-MD in uncracked oil (the "baseline concentration"), and Cc is the concentration in cracked oil). The definition criteria for baseline concentration should be integrated with the specific basin conditions. For instance, the Austin Chalk oil in South Texas has a baseline concentration of 7–10 ppm, whereas Upper Devonian oil from the Solimões Basin in Brazil has a concentration of 2–5 ppm (Dahl et al., 1999). Paleogene oil in the Dongying Sag and Paleozoic oil in the Tarim Basin have baseline concentrations of 20 ppm (Qiao et al., 2022, 2024a). More recent research has demonstrated that, at oil maturities between 1.2 % and 3.0 %, this formula will overestimate the cracking degree (Peng et al., 2022). The calculation formula from Dahl et al. (1999) was modified based on thermal simulation experiments: EOC2 = 1.2402 × EOC–28.952. The earlier formula had significant limitations due to constraints in petroleum exploration, whereas the revised formula is better suited for ultra-deep petroleum reservoirs (Wang et al., 2023; Qiao et al., 2024a, 2024b).

7.5. TSR

TSR is a series of REDOX reactions that occur when hydrocarbon organic matter interacts with sulfates at reservoir temperatures exceeding 130 °C (Cai et al., 2003, 2022; Machel et al., 1995). TSR can alter the $\delta^{13}C$ and molecular compositions of LHs. Whiticar and Snowdon (1999) analyzed oil samples from western Canada and found that *n*-paraffins were more susceptible to TSR than isoparaffins, cycloalkanes, and aromatics. The TSR process also leads to significant enrichment of ^{13}C in LHs.

Previous research has demonstrated that the K1 value in normal oil remains around 1.0 (Mango, 1997). However, under the influence of TSR, the K1 value in oil increases significantly, reaching values greater than 1.0 (Fig. 15; Cai et al., 2022; Song et al., 2017). Notably, the increase in the K1 value is not solely attributed to TSR. Previous studies have also reported high K1 values in coal-derived oils and saline lacustrine oils (Fig. 15; Wang et al., 2008; Wang and Zhang, 2008; Zhu et al., 2005). The K1 value should, therefore, be analyzed alongside other indicators for TSR identification, such as the content of dibenzothiophene series, thiadiamondoids, and sulfur isotopes (Cai et al., 2003). Other LH parameters that characterize secondary alteration processes are shown in Table 6.

8. Migration

Research on natural gas migration is primarily focused on isotope fractionation during migration (Zumberge et al., 2012; Schloemer and Krooss, 2004; Prinzhofer et al., 2000; Galimov, 1988). This results in the accumulation of ^{12}C at the migration endpoint as the migration distance increases. $\delta^{13}C_1$ is commonly used to trace natural gas migration (Wood et al., 2024; Kotarba and Lewan, 2013). Additional factors, such as thermal maturity, secondary alteration processes, and multi-stage charging, also influence $\delta^{13}C_1$.

During natural gas migration in a water-dissolving phase, the soluble components dissolve first. Early studies showed that, for the same carbon number, the solubility of paraffins, cycloalkanes, and aromatics

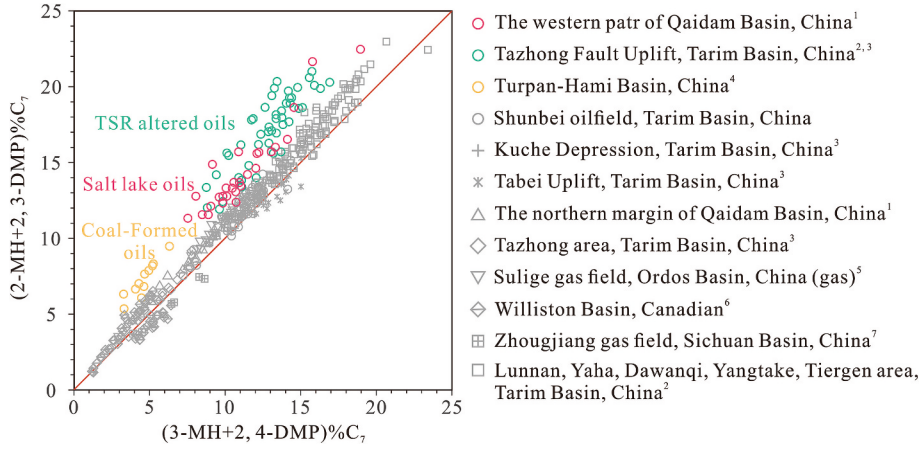

Fig. 15. Diagrams of (3MH + 2, 4DMP)%C_7 (MH: methylhexane; DMP: dimethylpentane) versus (2MH + 2, 3DMP)%C_7 (modified from Mango, 1987). Data 1 from Zhu et al., 2005; 2 from Zhang et al., 2005; 3 from Song et al., 2017; 4 from Wang and Zhang, 2008; 5 from Yu et al., 2014; 6 from Smith and Bend, 2004; and 7 from Wu et al., 2024b.

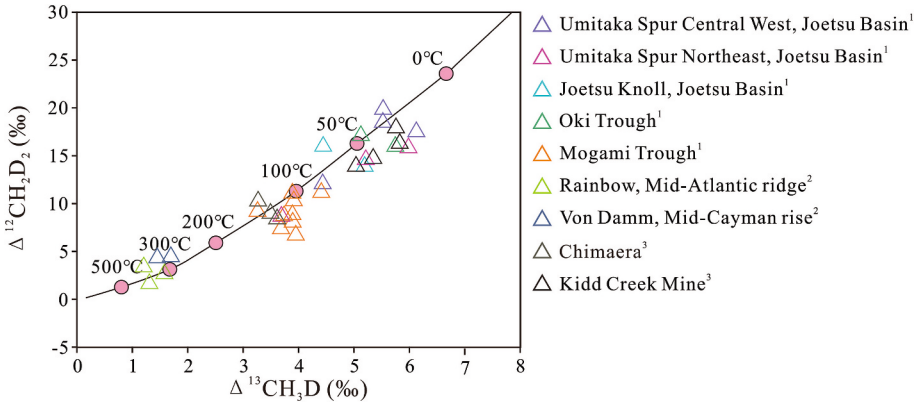

Fig. 16. Diagrams of $\Delta^{13}CH_3D$ (‰) versus $\Delta^{12}CH_2D_2$ (‰) (modified from Young et al., 2016). Data 1 from Zhang et al., 2021; 2 from Labidi et al., 2020; and 3 from Young et al., 2017.

increases progressively (Thompson, 1979). As the migration distance increases, the ratios of aromatic hydrocarbons to alkanes (e.g., Bz/nC_6, Tol/nC_7) and aromatic hydrocarbons to cycloalkanes (e.g., Bz/CH) in the water-dissolving phase increase (Huang et al., 2022). When natural gas migrates in its free gas phase, highly polar aromatic hydrocarbons are more readily adsorbed by rocks, leading to lower contents in the gas. Consequently, the ratios of Bz/nC_6, Tol/nC_7, and Bz/CH decrease with increasing migration distance (Table 6; Wu et al., 2024a; Yu et al., 2014, 2017).

The combined effects of secondary alterations significantly limit the use of LH parameters in oil migration tracing (Ricci et al., 2023; Cai et al., 2024). Other compound parameters offer better selection than LHs for oil migration tracing. These include carbazole, furan, dibenzothiophene, and the dibenzofuran series (Li et al., 2014, 2018b; Wang et al., 2004a).

9. The application of frontier technologies in light hydrocarbons

9.1. The application of clumped isotopes

The application of clumped isotopes is grounded in the thermodynamic effects of substitution between isotopologues (Eiler, 2007). At isotopic equilibrium, the concentrations of methane isotopologues (e.g., $^{13}CH_3D$ and $^{12}CH_2D_2$) depend solely on temperature, and they are in a functional relationship (Wang et al., 2004b). Clumped isotopes can determine the formation temperature of C_1 when C—H bonds are in equilibrium, offering significant potential for determining the formation temperature of natural gas (Fig. 16; Zhang et al., 2021; Young et al., 2016). If the order of isotopic bonds is in disequilibrium, the temperature of $^{13}CH_3D$ will be overestimated (Young et al., 2017). This could provide additional information about the methane cycle. For instance, isotopic imbalance in clusters can reveal dynamic isotope processes, including bond reordering, migration, oxidation, and mixing (Warr et al., 2021; Labidi et al., 2020). When using cluster isotopes to assess the formation temperature of C_1, it is crucial to account for potential dynamic processes. When methane is formed in near-surface environments with rapid rates, isotope dynamics may cause deviations from isotopic equilibrium, resulting in errors in the calculation of the natural gas formation temperature (Stolper et al., 2015). Methane cluster isotopes are also useful for distinguishing the mixing ratio between biogenic and thermogenic methane sources (Stolper et al., 2015).

Ethane (C_2) is a major alkane, second only to C_1 in natural gas. Clog et al. (2018) developed a method for measuring the $\Delta^{13}C_2H_6$ abundance in ethane using MAT 253 ultra mass spectrometry. It is pointed out that the C_2 cluster isotopic is primarily controlled by isotope dynamics and the inheritance of parent material in kerogen.

Cluster isotopes not only offer a novel method for studying gas isotopes but also offer deeper insights into the transformation processes and formation mechanisms of natural gas at the microscale. This is something that traditional organic geochemical methods cannot provide.

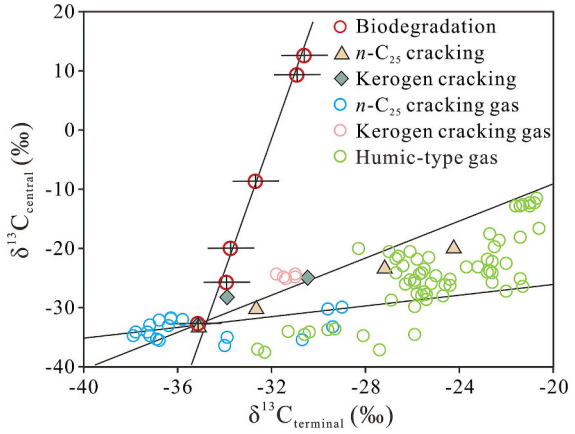

Fig. 17. Diagrams of $\delta^{13}C_{terminal}$ (‰) versus $\delta^{13}C_{central}$ (‰) (modified from Gilbert et al., 2019). (For details of the data sources, see Fig. A.10).

9.2. The application of PSIA

With developments in technology, the accurate determination of specific isotopes and the study of fractionation mechanisms have been widely used in the analysis of related scientific problems. The mechanisms of isotope fractionation can be categorized as thermodynamic fractionation and kinetic fractionation. The former is considered to be reversible and bi- or multi-directional, and the latter is generally irreversible, rapid, and incomplete. At present, the main application object of this technology in light hydrocarbons is propane. Webb and Miller (2014) employed the high-quality potential energy surfaces theory along with the Path Integral Monte Carlo Method (PIMC) to calculate the thermodynamic equilibrium of propane at a specific site. Subsequently, Piasecki et al. (2016b) applied the density probability function that is used to establish the thermodynamic equilibrium temperature and the relationship between $\delta^{13}C$ at various positions within the propane molecule. These studies provided a way to use position-specific isotopes of propane as a geothermometer. Subsequent studies have shown that the ΔC–T value ($\delta^{13}C_{central}$–$\delta^{13}C_{terminal}$) of propane in low-maturity natural gas is negative and increases markedly with maturity (Liu et al., 2019a, 2019b; Liu et al., 2023). Moreover, the difference between the two can indicate whether propane is derived from kerogen cracking

or the secondary cracking of asphalt/oil (Zhang et al., 2022).

Due to the kinetic isotope effect, microorganisms preferentially consume lighter isotopes, while heavier isotopes accumulate in the residual hydrocarbons. During biodegradation, the central carbon atom of propane is selectively activated by enzymes in anaerobic hydrocarbon oxidation. Therefore, during bacterial anaerobic oxidation, residual propane accumulates as ^{13}C in the central carbon, with the terminal carbon being less affected (Jaekel et al., 2014). Gilbert et al. (2019) demonstrated through simulation experiments that the carbon isotope ratio ($\delta^{13}C_{central}/\delta^{13}C_{terminal}$) of biogenic and thermogenic propane differs significantly, effectively distinguishing microbial from thermogenic gas (Fig. 17).

With the development and application of position-specific isotope analysis techniques, butane and larger hydrocarbon molecules have gradually come to be studied (Li et al., 2023; Julien et al., 2020), providing more evidence for the analysis of the origin and evolution of natural gas.

10. Future prospects

LHs, as key components of oil and gas, contain valuable geochemical information in their chemical and isotopic compositions. Recent advances in separation technology, isotopes, and high-resolution mass spectrometry analysis provide increasingly precise insights into the isotopic and chemical compositions of LHs. These advances offer novel perspectives for investigating petroleum formation and transformation processes. Despite extensive studies on the application of LHs, several challenges remain.

1. Current research on LHs primarily focuses on C_1-C_8 compounds. Although both quantitative and qualitative characterizations of C_8^+ LHs have been achieved in recent years, their overall development and application remain limited.
2. Generally, the isotopic fractionation effect of lower molecular weight hydrocarbons exceeds that of higher molecular weight hydrocarbons. As a result, the $\delta^{13}C$ of liquid-phase hydrocarbons (C_6-C_{13}) in LHs offers more reliable geochemical information. However, reports on their isotopic compositions are limited, and the development of isotopic parameters for related compounds has reached a standstill.
3. Regardless of GC-IRMS, PSIA, or clumped isotopes, there has been limited research on the hydrogen isotopes of LHs. Hydrogen isotopes experience greater isotopic fractionation than carbon isotopes during the oil and gas evolution process, potentially offering new insights for future research on the geneses and applications of LHs.

11. Conclusions

This study discusses the methods for identifying different modes of natural gas genesis based on the isotopic and chemical compositions of light hydrocarbons (LHs). Humic-type gas typically exhibits a heavier LH carbon isotope than sapropelic-type gas. During thermal evolution, oil-cracking gas and kerogen-cracking gas can be effectively distinguished according to the differing formation rates of LH components. Biodegradation results in lighter carbon isotopes and abnormal enrichment of methane. Current organic geochemical methods are ineffective for distinguishing between primary microbial gas-F and primary microbial gas-CR. The distinction between the two relies more on a comprehensive analysis of the geological evolution context. Notably, current genetic identification methods have limitations in distinguishing gases with mixed geneses.

LHs originating from sapropelic-type source rocks contain abundant *n*-paraffins, while those from humic types have higher contents of isoparaffins and cycloalkanes. Furthermore, differences in the hydrogen isotopic compositions of LHs ($\Delta\delta D_{Tol\text{-}MCH}$ and $\Delta\delta D_{nC7\text{-}Tol}$) can effectively distinguish the depositional environments of their source rocks.

Ethane typically undergoes isotopic inversion during thermal evolution, making it unsuitable for natural gas maturity assessment. The empirical maturity formula, based on methane carbon isotopes, effectively evaluates the maturity of both humic-type gas and sapropelic-type gas. However, this formula does not apply to mixed gas. The heptane value, isoheptane value, and methyldiamantane index serve as useful indicators for evaluating oil maturity, although secondary alteration effects must be considered in their application.

In newly formed light oils, the concentration of low-molecular-weight diamondoids (e.g., (1- + 2-) MA) and *n*-paraffins increases, while the aromatic content decreases during evaporative fractionation. In contrast, the residual oil exhibits the opposite trends. Water washing also reduces the aromatic contents in both oil and gas. The structure and carbon numbers of LHs influence their susceptibility to biodegradation. Under intense biodegradation (PM $\geq$ 4), most LHs are degraded. Biodegradation also causes the $\delta^{13}C_1$ to become lighter and the $\delta^{13}C$ of the heavy hydrocarbon components to become heavier. Both baseline concentration selection and the potential influences of TSR and evaporative fractionation must be considered when using diamondoids to assess the degree of oil cracking. TSR typically causes the $\delta^{13}C$ of LHs to become heavier, also resulting in K1 values significantly greater than 1.0. However, K1 values greater than 1.0 are not exclusive to TSR.

The ratios of aromatic to *n*-paraffins and cycloalkanes increase with migration distance when natural gas migrates as a water-dissolving phase. In contrast, when natural gas migrates as a free gas phase, these parameters decrease with increasing migration distance. However, using LH parameters for oil migration tracing presents certain limitations.

In general, the chemical and isotopic compositions of LHs are crucial for identifying the sources and origins of hydrocarbons, their depositional environments, the maturity of their corresponding source rocks, gas formation temperatures, migration directions, and secondary alteration processes. However, there are a number of specific limitations. Recent advances in ultra-deep petroleum exploration and emerging analytical technologies have significantly expanded the application potential of LH parameters.

Declaration of competing interest

The authors declare that they have no known competing financial interests or personal relationships that could have appeared to influence the work reported in this paper.

Acknowledgments

This work was funded by the National Natural Science Foundation of China (Grant No. 42173054). The author expresses gratitude to the co-editors-in-chief, Massimo Zecchin, reviewer B. J. Katz, and the one anonymous reviewer for their valuable and constructive reviews, which have significantly enhanced the manuscript.

Appendix A. Supplementary data

Supplementary data to this article can be found online at https://doi.org/10.1016/j.earscirev.2025.105164.

Data availability

Data will be made available on request.

References

Abelson, P.H., Hoering, T.C., 1961. Carbon isotope fractionation in formation of amino acids by photosynthetic organisms. Proc. Nat. Acad. Sci. USA 47 (5), 623–632.
Abrajano, T.A., Sturchio, N.C., Bohlke, J.K., Lyon, G.L., Poreda, R.J., Stevens, C.M., 1988. Methane-hydrogen gas seeps, Zambales Ophiolite, Philippines: deep or shallow origin? Chem. Geol. 71 (1–3), 211–222.

Abrams, M.A., Thomas, D., 2020. Geochemical evaluation of oil and gas samples from the Upper Devonian and Mississippian reservoirs Southern Anadarko Basin Oklahoma and its implication for the Woodford Shale unconventional play. Mar. Pet. Geol. 112, 104043.
Aguiar, A., Silva Júnior, A.I., Azevedo, D.A., Aquino Neto, F.R., 2010. Application of comprehensive two-dimensional gas chromatography coupled to time-of-flight mass spectrometry to biomarker characterization in Brazilian oils. Fuel 89 (10), 2760–2768.
Bahaghighat, H.D., Freye, C.E., Synovec, R.E., 2019. Recent advances in modulator technology for comprehensive two dimensional gas chromatography. TrAC Trends Anal. Chem. 113, 379–391.
Behar, F., Ungerer, P., Kressmann, S., Rudkiewicz, J.L., 1991. Thermal Evolution of crude oils in Sedimentary Basins: Experimental simulation in a Confined System and Kinetic Modeling. Oil Gas Sci. Technol. Revue de l IFP 46 (2), 151–181.
Behar, F., Kressmann, S., Rudkiewicz, J.L., Vandenbroucke, M., 1992. Experimental simulation in a confined system and kinetic modelling of kerogen and oil cracking. Org. Geochem. 19 (1–3), 173–189.
Behar, F., Vandenbroucke, M., Teermann, S.C., Hatcher, P.G., Leblond, C., Lerat, O., 1995. Experimental simulation of gas generation from coals and a marine kerogen. Chem. Geol. 126 (3–4), 247–260.
Bernard, B.B., Brooks, J.M., Sackett, W.M., 1977. A geochemical model for characterization of hydrocarbon gas sources in marine sediments. In: Offshore Technology Conference.
Bernard, B.B., Brooks, J.M., Sackett, W.M., 1978. Light hydrocarbons in recent Texas continental shelf and slope sediments. J. Geophys. Res. Oceans 83, 4053–4061.
Berner, U., Faber, E., 1996. Empirical carbon isotope/maturity relationships for gases from algal kerogens and terrigenous organic matter, based on dry, open-system pyrolysis. Org. Geochem. 24 (10−11), 947–955.
Berner, U., Faber, E., Scheeder, G., Panten, D., 1995. Primary cracking of algal and landplant kerogens: Kinetic models of isotope variations in methane, ethane, and propane. Chem. Geol. 126 (3–4), 233–245.
Bjorøy, M., Hall, P.B., Moe, R.P., 1994. Variation in the isotopic composition of single components in the C_4–C_{20} fraction of oils and condensates. Org. Geochem. 21 (6–7), 761–776.
Boreham, C.J., Golding, S.D., Glikson, M., 2001. Reply to comment of Smith and Pallaser on factors controlling the origin of gas in Australian Bowen Basin coals. Org. Geochem. 32, 207–210.
Brown, A., 2011. Identification of source carbon for microbial methane in unconventional gas reservoirs. AAPG Bull. 95 (8), 1321–1338.
Cai, C.F., Hu, W.S., Worden, R.H., 2001. Thermochemical sulphate reduction in Cambro–Ordovician carbonates in Central Tarim. Mar. Pet. Geol. 18 (6), 729–741.
Cai, C.F., Worden, R.H., Bottrell, S.H., Wang, L.S., Yang, C.C., 2003. Thermochemical sulphate reduction and the generation of hydrogen sulphide and thiols (mercaptans) in Triassic carbonate reservoirs from the Sichuan Basin. China. Chemical Geology 202 (1–2), 39–57.
Cai, C.F., Xiao, Q.L., Fang, C.C., Wang, T.K., He, W.X., Li, H.X., 2016. The effect of thermochemical sulfate reduction on formation and isomerization of thiadiamondoids and diamondoids in the lower Paleozoic petroleum pools of the Tarim Basin, NW China. Org. Geochem. 101, 49–62.
Cai, C.F., Li, H.X., Li, K.K., Wang, D.W., 2022. Thermochemical sulfate reduction in sedimentary basins and beyond: A review. Chem. Geol. 607, 121018.
Cai, S.Y., Xiao, Q.L., Cheng, T., She, J.C., Chen, S.P., Yang, X., 2024. Molecular and stable carbon isotopic compositions of crude oils from Shengbei Sag, Tuha Basin: Implications for hydrocarbon sources, migration and mixing. Fuel 371, 131877.
Cañipa-Morales, N.K., Galán-Vidal, C.A., Guzmán-Vega, M.A., Jarvie, D.M., 2003. Effect of evaporation on C_7 light hydrocarbon parameters. Org. Geochem. 34 (6), 813–826.
Cesar, J., Nightingale, M., Becker, V., Mayer, B., 2020. Stable carbon isotope systematics of methane, ethane and propane from low-permeability hydrocarbon reservoirs. Chem. Geol. 558, 119907.
Chang, X.C., Mao, L.X., Xu, Y.D., Li, T.T., 2017. C_8 Light Hydrocarbon Parameters to Indicate Source Facies and thermal Maturity Characterized by Comprehensive Two-Dimensional Gas Chromatography. Energy Fuel 31 (9), 9223–9231.
Chang, Z.Y., Zhang, W.F., Ge, X., Zhu, S.K., 2018. Use of light hydrocarbons for the oil-oil correlation in Pearl River Mouth Basin, South China Sea. Fuel 221, 179–187.
Charlou, J.L., Fouquet, Y., Bougault, H., Donval, J.P., Etoubleau, J., Jean-Baptiste, P., Dapoigny, A., Appriou, P., Rona, P.A., 1998. Intense CH_4 plumes generated by serpentinization of ultramafic rocks at the intersection of the 15°20′N fracture zone and the Mid-Atlantic Ridge. Geochim. Cosmochim. Acta 62 (13), 2323–2333.
Chen, J.H., Fu, J.M., Sheng, G.Y., Liu, D.H., Zhang, J.J., 1996. Diamondoid hydrocarbon ratios: novel maturity indices for highly mature crude oils. Org. Geochem. 25 (3–4), 179–190.
Chen, J.F., Miao, Z.Y., Zhang, C., Chen, H.Y., 2010. Geochemical chariacteristics of light hydrocarbons in natural gas in the Tabei Uplift of the Tarim Basin and their implications. Oil Gas Geol. 31 (3), 271–276 (In Chinese).
Chen, J.J., Zhao, J.Z., Li, J., Cao, Q., Wang, Z., 2020. Geochemical Characteristics of Upper Paleozoic Natural Gas in Southern Ordos Basin: A Case Study of Zhidan-Ganquan Area. Sci. Technol. Eng. 20 (26), 10598–10604 (In Chinese).
Chen, J.P., Wang, X.L., Chen, J.F., Ni, Y.Y., Xiang, B.L., Liao, F.R., He, W.J., Yao, L.M., Li, E.T., 2021. New equation to decipher the relationship between carbon isotopic composition of methane and maturity of gas source rocks. Sci. China Earth Sci. 64, 470–493.
Chen, X.Y., Liu, W.H., Cao, Y.J., Yin, J., Guo, L.X., Wang, X.F., Zhang, D.D., Zhang, J., Luo, H.Y., 2022. Natural gas origin of Langgu Sag in Jizhong Depression, Bohai Bay Basin: Insight from hydrous pyrolysis experiments of gold tube. J. Nat. Gas Sci. Eng. 103, 104610.
Cheng, B., Wang, T.G., Huang, H.P., Wang, G.L., 2015a. Application of the monoterpane ratio (MTR) to distinguish marine oils from terrigenous oils and infer depositional environment in northern Tarim Basin, China. Org. Geochem. 85, 1–10.
Cheng, B., Wang, T.G., Huang, H.P., Wang, G.L., Simoneit, B.R.T., 2015b. Ratios of low molecular weight alkylbenzenes (C_0–C_4) in Chinese crude oils as indicators of maturity and depositional environment. Org. Geochem. 88, 78–90.
Cheng, B., Liang, Y.G., Xu, J.B., Deng, Q., Wei, Z.W., Faboya, O.L., Liao, Z.W., 2018. Remarkable Fractionation of the Hydrogen Isotope (δD) of Hydrocarbon during the Fast Aromatization Process: Insights from the Pyrolysis experiments of *n*-Butylcyclohexane. ACS Earth Space Chem. 2, 1240–1248.
Clayton, J.L., Rice, D.D., Michael, G.E., 1991. Oil-generating coals of the San Juan Basin, New Mexico and Colorado, U.S.A. Org. Geochem. 17 (6), 735–742.
Clog, M., Lawson, M., Peterson, B., Ferreira, A.A., Santos Neto, E.V., Eiler, J.M., 2018. A reconnaissance study of ^{13}C–^{13}C clumping in ethane from natural gas. Geochim. Cosmochim. Acta 223 (15), 229–244.
Coleman, D.D., Bruno Risatti, J., Schoell, M., 1981. Fractionation of carbon and hydrogen isotopes by methane-oxidizing bacteria. Geochim. Cosmochim. Acta 45 (7), 1033–1037.
Corso, T.N., Brenna, J.T., 1997. High-precision position-specific isotopeanalysis. PNAS 94 (4), 1049–1053.
Coudrain-Ribstein, A., Gouze, P., De Marsily, G., 1998. Temperature-carbon dioxide partial pressure trends in confined aquifers. Chem. Geol. 145 (1–2), 73–89.
Dahl, J.E., Moldowan, J.M., Peters, K.E., Claypool, G.E., Rooney, M.A., Michael, G.E., Mello, M.R., Kohnen, M.L., 1999. Diamondoid hydrocarbons as indicators of natural oil cracking. Nature 399, 54–57.
Dai, J.X., 1992. Identification and distinction of various alkane gases. Sci. Sin. Chim. 35, 1246–1257 (In Chinese).
Dai, J.X., Li, P.J., 1994. The study on carbon isotope composition of C_5–C_8 light hydrocarbons in the natural gases from the main oil & gas bearing basins, China. Chin. Sci. Bull. 39 (22), 2071–2073 (In Chinese).
Dai, J.X., Song, Y., Guan, D.S., Gan, L.D., 1987. Identification of coal-derived gas. In: Study on Coal–Derived Gas Geology Symposium (in Chinese). Petroleum Industry Press, Beijing, pp. 156–170.
Dai, J.X., Xia, X.Y., Qin, S.F., Zhao, J.Z., 2004. Origins of partially reversed alkane $\delta^{13}C$ values for biogenic gases in China. Org. Geochem. 35 (4), 405–411.
Dai, J.X., Yang, S.F., Chen, H.L., Shen, X.H., 2005. Geochemistry and occurrence of inorganic gas accumulations in Chinese sedimentary basins. Org. Geochem. 36 (12), 1664–1688.
Dai, J.X., Zou, C.N., Zhang, S.C., Li, J., Ni, Y.Y., Hu, G.Y., Luo, X., Tao, S.Z., Zhu, G.Y., Mi, J.K., Li, Z.S., Hu, A.P., Yang, C., Zhou, Q.H., Shuai, Y.H., Zhang, Y., Ma, C.H., 2008. Discrimination of abiogenic and biogenic alkane gases. Sci. China Ser. D Earth Sci. 51, 1737–1749.
Dai, J.X., Ni, Y.Y., Huang, S.P., Liao, F.R., Yu, C., Gong, D.Y., Wu, W., 2014. Significant function of Coal–derived gas study for natural gas industry development in China. Nat. Gas Geosci. 25 (1), 1–22 (In Chinese).
Dai, J.X., Ni, Y.Y., Huang, S.P., Gong, D.Y., Liu, D., Feng, Z.Q., Peng, W.L., Han, W.X., 2016. Secondary origin of negative carbon isotopic series in natural gas. J. Nat. Gas Geosci. 1 (1), 1–7.
Dallüge, J., Vreuls, R.J.J., Beens, J., Brinkman, U.A.T., 2002. Optimization and characterization of comprehensive two-dimensional gas chromatography with time-of-flight mass spectrometric detection (GC×GC–TOF MS). J. Sep. Sci. 25 (4), 201–214.
Deng, H.Y., Zhang, H.Z., Zhang, Y.M., Chen, N.D., Mo, T., Cheng, B., Liao, Z.W., 2023. Genetic identification of light oils and condensates using δD indices of C_7 hydrocarbons: A case study in the Tarim Basin, NW China. Int. J. Coal Geol. 279, 104372.
Douglas, P.M.J., Stolper, D.A., Eiler, J.M., Sessions, A.L., Lawson, M., Shuai, Y.H., Shuai, A., Podlaha, O.G., Podlaha, A.A., Santos Neto, E.V., Niemann, M., Steen, A.S., Huang, L., Chimiak, L., Valentine, D.L., Fiebig, J., Fiebig, A.J., Seyfried Jr., W.E., Etiope, G., Schoell, M., Inskeep, W.P., Moran, J.J., Kitchen, N., 2017. Methane clumped isotopes: Progress and potential for a new isotopic tracer. Org. Geochem. 113, 262–282.
Dzou, L.I., 2010. Kuparuk oil field, Alaska, a mixture of Kekiktuk gas condensate and Shublik oil. AAPG Bull. 94 (11), 1761–1778.
Dzou, L.I.P., Hughes, W.B., 1993. Geochemistry of oils and condensates, K Field, offshore Taiwan: a case study in migration fractionation. Org. Geochem. 20 (4), 437–462.
Eiler, J.M., 2007. "Clumped-isotope" geochemistry—the study of naturally-occurring, multiply-substituted isotopologues. Earth Planet. Sci. Lett. 262, 309–327.
Eiler, J.M., 2013. The Isotopic Anatomies of Molecules and Minerals. Annu. Rev. Earth Planet. Sci. 41, 411–441.
Eiler, J.M., Schauble, E., 2004. $^{18}O^{13}C^{16}O$ in Earth's atmosphere. Geochim. Cosmochim. Acta 68 (23), 4767–4777.
Faber, E., 1987. Zur Isotopengeochemie gasförmiger Kohlenwasserstoffe. Erdöl, Erdgas, Kohle 103 (5), 210–218.
Faramawy, S., Zaki, T., Sakr, A.A.E., 2016. Natural gas origin, composition, and processing: A review. J. Nat. Gas Sci. Eng. 34, 34–54.
Farrimond, P., Taylor, A., TelnÆs, N., 1998. Biomarker maturity parameters: the role of generation and thermal degradation. Org. Geochem. 29 (5–7), 1181–1197.
Forziati, A.F., Willingham, C.B., Mair, B.J., Rossini, F.D., 1944. Hydrocarbons in the gasoline fraction of seven representative crudes, including all the distillate to 102°C and the aromatics to 160°C. J. Res. Natl. Bur. Stand. 32, 11–37.
Fu, R., 2023. Geochemical Characteristics and Geological Significance of Deep gas in the Central Sichuan Basin. China University of Petroleum, Beijing (In Chinese).
Fuex, A.N., 1977. The use of stable carbon isotopes in hydrocarbon exploration. J. Geochem. Explor. 7, 155–188.

Galimov, E.M., 1988. Sources and mechanisms of formation of gaseous hydrocarbons in sedimentary rocks. Chem. Geol. 71 (1–3), 77–95.
Gao, L., He, P.Q., Jin, Y.B., Zhang, Y.Q., Wang, X.Q., Zhang, S.C., Tang, Y.C., 2016. Determination of position-specific carbon isotope ratios in propane from hydrocarbon gas mixtures. Chem. Geol. 435, 1–9.
Gao, J.L., Liu, J.Q., Ni, Y.Y., 2018. Gas generation and its isotope composition during coal pyrolysis: the catalytic effect of nickel and magnetite. Fuel 222, 74–82.
George, S.C., Boreham, C.J., Minifie, S.A., Teerman, S.C., 2002. The effect of minor to moderate biodegradation on C_5 to C_9 hydrocarbons in crude oils. Org. Geochem. 33 (12), 1293–1317.
Gilbert, A., Yamada, K., Yoshida, N., 2013. Exploration of intramolecular ^{13}C isotope distribution in long chain n-alkanes (C_{11}–C_{31}) using isotopic ^{13}C NMR. Org. Geochem. 62, 56–61.
Gilbert, A., Yamada, K., Suda, K., Ueno, Y., Yoshida, N., 2016. Measurement of position-specific ^{13}C isotopic composition of propane at the nanomole level. Geochim. Cosmochim. Acta 177, 205–216.
Gilbert, A., Sherwood Lollar, B., Musat, F., Giunta, T., Chen, S.C., Kajimoto, Y., Yamada, K., Boreham, C.J., Yoshida, N., Ueno, Y., 2019. Intramolecular isotopic evidence for bacterial oxidation of propane in subsurface natural gas reservoirs. Pans 116 (14), 6653–6658.
Golding, S.D., Boreham, C.J., Esterle, J.S., 2013. Stable isotope geochemistry of coal bed and shale gas and related production waters: A review. Int. J. Coal Geol. 120, 24–40.
Gong, D.Y., Cao, Z.L., Ni, Y.Y., Jiao, L.X., Yang, B., Zhao, L.L., 2016. Origins of Jurassic oil reserves in the Turpan–Hami Basin, northwest China: Evidence of admixture from source and thermal maturity. J. Pet. Sci. Eng. 146, 788–802.
Halpern, H.I., 1995. Development and applications of Light-Hydrocarbon-based Star Diagrams. AAPG Bull. 79 (6), 801–815.
Hartgers, W.A., Sinninghe Damsté, J.S., de Leeuw, J.W., 1994. Geochemical significance of alkylbenzene distributions in flash pyrolysates of kerogens, coals, and asphaltenes. Geochim. Cosmochim. Acta 58 (7), 1759–1775.
Hayes, J.M., Freeman, K.H., Popp, B.N., Hoham, C.H., 1990. Compound-specific isotopic analyses: A novel tool for reconstruction of ancient biogeochemical processes. Org. Geochem. 16 (4–6), 1115–1128.
He, K., Zhang, S.C., Mi, J.K., Zhang, W.L., 2018. Pyrolysis involving n-hexadecane, water and minerals: Insight into the mechanisms and isotope fractionation for water-hydrocarbon reaction. J. Anal. Appl. Pyrolysis 130, 198–208.
Henkes, G.A., Passey, B.H., Grossman, E.L., Shenton, B.J., Yancey, T.E., Pérez-Huerta, A., 2018. Temperature evolution and the oxygen isotope composition of Phanerozoic oceans from carbonate clumped isotope thermometry. Earth Planet. Sci. Lett. 490 (15), 40–50.
Hill, R.J., Tang, Y.C., Kaplan, I.R., 2003. Insights into oil cracking based on laboratory experiments. Org. Geochem. 34 (12), 1651–1672.
Hill, R.J., Lu, S., Tang, Y., Henry, M., Kaplan, I.R., 2004. C_4-benzene and C_4-naphthalene thermal maturity indicators for pyrolysates, oils and condensates. Geochem. Soc. Spec. Publ. 9, 303–319.
Hou, D.J., Wang, P.R., Lin, R.Z., Li, S.J., 1989. Light hydrocarbons in pyrolysis gas of Maoming oil shale and its thermal evolution significance. J. Oil Gas Technol. 11 (4), 7–11 (In Chinese).
Hu, T.L., Ge, B.X., Zhang, Y.G., Liu, B., 1990. The development and application of fingerprint parameters for hydrocarbons absorbed by source rocks and light hydrocarbons in natural gas. Pet. Geol. Exp. 12 (4), 375–394 (In Chinese).
Hu, G.Y., Li, J., Li, J., Li, Z.S., Luo, X., Sun, Q.W., Ma, C.H., 2007. Discussion on the light hydrocarbons index in the identification of natural gas. Sci. Sin. Terrae 37 (1), 111–117 (In Chinese).
Huang, S.P., Fang, C.C., Peng, W.L., Jiang, Q.C., Feng, Z.Q., 2017. Stable carbon isotopic composition of light hydrocarbons and *n*-alkanes of condensates in the Tarim Basin, NW China. J. Nat. Gas Geosci. 2 (3), 165–177.
Huang, S.P., Li, J.Z., Wang, T.S., Jiang, Q.C., Jiang, H., Tao, X.W., Bai, B., Feng, Z.Q., 2022. Application of Light Hydrocarbons in Natural Gas Geochemistry of Gas Fields in China. Annu. Rev. Earth Planet. Sci. 50, 13–53.
Hunt, J.M., 1975. Origin of gasoline range alkanes in the deep sea. Nature 254 (5499), 411–413.
Hunt, J.M., 1984. Generation and Migration of Light Hydrocarbons. Science 226 (4680), 1265–1270.
Hunt, J.M., Huc, A.Y., Whelan, J.K., 1980. Generation of light hydrocarbons in sedimentary rocks. Nature 288 (5792), 688–690.
Jaekel, U., Vogt, C., Fischer, A., Richnow, H.-H., Musat, F., 2014. Carbon and hydrogen stable isotope fractionation associated with the anaerobic degradation of propane and butane by marine sulfate-reducing bacteria. Environ. Microbiol. 16, 130–140.
James, A.T., Martin, A.J.P., 1952. Gas-liquid partition chromatography: the separation and micro-estimation of volatile fatty acids from formic acid to dodecanoic acid. Biochem. J. 50 (5), 679–690.
Jenden, P.D., Kaplan, I.R., Poreda, R., Craig, H., 1988. Origin of nitrogen-rich natural gases in the California Great Valley: evidence from helium, carbon and nitrogen isotope ratios. Geochim. Cosmochim. Acta 52 (4), 851–861.
Jenden, P.D., Kaplan, I.R., Hilton, D.R., Craig, H., 1993. Abiogenic hydrocarbons and mantle helium in oil and gas fields. U. S. Geol. Surv. Prof. Pap. 1570, 31–56.
Jiang, M.M., Liu, Q.Y., 2025. Geochemical characteristics of ultra-deep natural gases. Org. Geochem. 203, 104964.
Jiang, Z.S., Luo, X., Li, Z.S., Zhang, Y., Pan, X.Z., 2000. Carbon isotope composition of benzene and toluene as a new index for correlation of gases with their source rocks. Geochimica 29 (4), 410–415 (In Chinese).
Jiang, M.M., Liu, Q.Y., Wu, X.Q., Zhu, D.Y., 2025. Advancements in geochemistry and origins of CO2 in natural gas reservoirs of China. Mar. Pet. Geol. 173, 107267.
Jones, D.M., Head, I.M., Gray, N.D., Adams, J.J., Rowan, A.K., Aitken, C.M., Bennett, B., Huang, H., Brown, A., Bowler, B.F.J., Oldenburg, T., Erdmann, M., Larter, S.R., 2008. Crude-oil biodegradation via methanogenesis in subsurface petroleum reservoirs. Nature 451, 176–180.
Julien, M., Goldman, M.J., Liu, C.J., Horita, J., Boreham, C.J., Yamada, K., Green, W.H., Yoshida, N., Gilbert, A., 2020. Intramolecular ^{13}C isotope distributions of butane from natural gases. Chem. Geol. 541, 119571.
Kang, X., Hu, W.X., Tan, J.Q., Li, Z.P., Xiang, B., Wang, J., Wang, X.L., 2021. Hydrogen isotopic responses to thermochemical oxidation of light hydrocarbon gases in deep clastic reservoirs of the Junggar Basin, China. Chem. Geol. 563, 120052.
Katz, B.J., 2011. Microbial Processes and Natural Gas Accumulations. Open Geol. J. 5 (1), 75–83.
Katz, B.J., Narimanov, A., Huseinzadeh, R., 2002. Significance of microbial processes in gases of the South Caspian basin. Mar. Pet. Geol. 19 (6), 783–796.
Khairy, A., El Diasty, W.S., Peters, K.E., Meredith, W., 2022. Molecular and isotopic evidence for the origin of light oils and associated gases in the onshore Northeast Nile Delta. Mar. Pet. Geol. 140, 105658.
Koopmans, M.P., Köster, J., Van Kaam-Peters, H.M.E., Kenig, F., Schouten, S., Hartgers, W.A., de Leeuw, J.W., Sinninghe Damsté, J.S., 1996. Diagenetic and catagenetic products of isorenieratene: Molecular indicators for photic zone anoxia. Geochim. Cosmochim. Acta 60 (22), 4467–4496.
Kotarba, M.J., Lewan, M.D., 2013. Sources of natural gases in Middle Cambrian reservoirs in polish and Lithuanian Baltic Basin as determined by stable isotopes and hydrous pyrolysis of lower Palaeozoic source rocks. Chem. Geol. 345, 62–76.
Labidi, J., Young, E.D., Giunta, T., Kohl, I.E., Seewald, J., Tang, H., Lilley, M.D., Früh-Green, G.L., 2020. Methane thermometry in deep-sea hydrothermal systems: evidence for re-ordering of doubly-substituted isotopologues during fluid cooling. Geochim. Cosmochim. Acta 288, 248–261.
Lafargue, E., Le Thiez, P., 1996. Effect of waterwashing on light ends compositional heterogeneity. Org. Geochem. 24 (12), 1141–1150.
Lancet, M.S., Andets, E., 1970. Carbon isotope fractionation in the Lancet the Fischer-Tropsch synthesis and in meteorites. Science 170 (3961), 980–982.
Larter, S., di Primio, R., 2005. Effects of biodegradation on oil and gas field PVT properties and the origin of oil rimmed gas accumulations. Org. Geochem. 36 (2), 299–310.
Leythaeuser, D., Schaefer, R.G., Cornford, C., Weiner, B., 1979. Generation and migration of light hydrocarbons (C_2–C_7) in sedimentary basins. Org. Geochem. 1 (4), 191–204.
Li, J.G., Paul, P., Cui, M.Z., 2000. Methyl diamantane index (MDI) as a maturity parameter for lower Palaeozoic carbonate rocks at high maturity and overmaturity. Org. Geochem. 31 (4), 267–272.
Li, G.Z., Hu, B., Deng, T.L., Yuan, Z.Y., 2007. Analytic techniques and petroleum geological significance of different existing states of light hydrocarbons. Nat. Gas Geosci. 18 (1), 111–116 (In Chinese).
Li, M.J., Wang, T.G., Shi, S.B., Liu, K.Y., Ellis, G.S., 2014. Benzo[b]naphthothiophenes and alkyl dibenzothiophenes: Molecular tracers for oil migration distances. Mar. Pet. Geol. 57, 403–417.
Li, Y., Zhang, L., Xiong, Y.Q., Gao, S.T., Yu, Z.Q., Peng, P.A., 2018a. Determination of position-specific carbon isotope ratios of propane from natural gas. Org. Geochem. 119, 11–21.
Li, M.J., Liu, X.Q., Wang, T.G., Jiang, W.D., Fang, R.H., Yang, L., Tang, Y.J., 2018b. Fractionation of dibenzofurans during subsurface petroleum migration: based on molecular dynamics simulation and reservoir geochemistry. Org. Geochem. 115, 220–232.
Li, X.Q., McGovern, G.P., Horita, J., 2021. Kinetics of propane cracking and position-specific isotope fractionation: Insights into the origins of natural gases. Org. Geochem. 155, 104234.
Li, X.Q., Xie, H., Birdwell, J.E., McGovern, G.P., Horita, J., 2023. Intramolecular carbon isotope geochemistry of butane isomers from laboratory maturation and Monte-Carlo simulations of kerogen types I, II, and III. Geochim. Cosmochim. Acta 360, 57–67.
Liang, Q.Y., Xiong, Y.Q., Zhao, J., Fang, C.C., Li, Y., 2017. Carbon isotopic fractionation during vaporization of low molecular weight hydrocarbons (C_6–C_{12}). Pet. Sci. 14, 302–314.
Liang, G., Gan, J., You, J.J., Li, X., Lei, M.Z., 2020. Geochemical characteristics and exploration prospect of low mature coal-derived gas in Qiongdongnan Basin. Nat. Gas Geosci. 31 (7), 895–903 (In Chinese).
Liu, R.B., 2015. Typical features of the first giant shale gas field in China. Nat. Gas Geosci. 26 (8), 1488–1498 (In Chinese).
Liu, Z.Y., Phillips, J.B., 1991. Comprehensive Two-Dimensional Gas Chromatography using an On-Column thermal Modulator Interface. J. Chromatogr. Sci. 29 (6), 227–231.
Liu, W.H., Xu, Y.C., 1999. A two-stage model of carbon isotopic fractionation in coal-gas. Geochimica 28 (4), 359–366 (in chinese).
Liu, Q.Y., Dai, J.X., Jin, Z.J., Li, J., Wu, X.Q., Meng, Q.Q., Yang, C., Zhou, Q.H., Feng, Z. H., Zhu, D.Y., 2016. Abnormal carbon and hydrogen isotopes of alkane gases from the Qingshen gas field, Songliao Basin, China, suggesting abiogenic alkanes? J. Asian Earth Sci. 115, 285–297.
Liu, Q.Y., Jin, Z.J., Li, H.L., Wu, X.Q., Tao, X.W., Zhu, D.Y., Meng, Q.Q., 2018a. Geochemistry characteristics and genetic types of natural gas in central part of the Tarim Basin, NW China. Mar. Petrol. Geol. 89 (1), 91–105.
Liu, C.J., McGovern, G.P., Liu, P., Zhao, H., Horita, J., 2018b. Position-specific carbon and hydrogen isotopic compositions of propane from natural gases with quantitative NMR. Chem. Geol. 491, 14–26.
Liu, C.J., Liu, P., McGovern, G.P., Horita, J., 2019a. Molecular and intramolecular isotope geochemistry of natural gases from the Woodford Shale, Arkoma Basin, Oklahoma. Geochim. Cosmochim. Acta 255, 188–204.

Liu, Q.Y., Wu, X.Q., Wang, X.F., Jin, Z.J., Zhu, D.Y., Meng, Q.Q., Huang, S.P., Liu, J.Y., Fu, Q., 2019b. Carbon and hydrogen isotopes of methane, ethane, and propane: A review of genetic identification of natural gas. Earth Sci. Rev. 190, 247–272.
Liu, Q.Y., Wu, X.Q., Zhu, D.Y., Meng, Q.Q., Xu, H.Y., Peng, W.L., Huang, X.W., Liu, J.Y., 2021. Generation and resource potential of abiogenic alkane gas under organic-inorganic interactions in petroliferous basins. J. Nat. Gas Geosci. 6 (2), 79–87.
Liu, P., Wang, X.F., Liu, C.J., Liu, W.H., 2023. Kinetic isotope effect and reaction pathways of thermogenic propane generation at early maturation stage: Insights from position-specific carbon isotope distribution. Mar. Pet. Geol. 153, 106252.
Liu, Q.Y., Wei, Y.B., Li, P.P., Huang, X.W., Meng, Q.Q., Wu, X.Q., Zhu, D.Y., Xu, H.Y., Fu, Y., Zhu, D., Zhang, W., Jin, Z.J., 2025. Natural hydrogen in the volcanic-bearing sedimentary basin: Origin, conversion, and production rates. Sci. Adv. 11 (4), eadr6771.
Losh, S., Cathles, L., Meulbroek, P., 2002. Gas washing of oil along a regional transect, offshore Louisiana. Org. Geochem. 33 (6), 655–663.
Machel, H.G., Roy Krouse, H., Sassen, R., 1995. Products and distinguishing criteria of bacterial and thermochemical sulfate reduction. Appl. Geochem. 10 (4), 373–389.
Mango, F.D., 1987. An Invariance in the Isoheptanes of Petroleum. Science 237 (4814), 514–517.
Mango, F.D., 1990. The origin of light hydrocarbons in petroleum: A kinetic test of the steady-state catalytic hypothesis. Geochim. Cosmochim. Acta 54 (5), 1315–1323.
Mango, F.D., 1994. The origin of light hydrocarbons in petroleum: Ring preference in the closure of carbocyclic rings. Geochim. Cosmochim. Acta 58 (2), 895–901.
Mango, F.D., 1997. The light hydrocarbons in petroleum: a critical review. Org. Geochem. 26 (7–8), 417–440.
Mango, F.D., 2000. The origin of light hydrocarbons. Geochim. Cosmochim. Acta 64 (7), 1265–1277.
Masterson, D.W., Dzou, L.I.P., Holba, A.G., Fincannon, A.L., Ellis, L., 2001. Evidence for biodegradation and evaporative fractionation in West Sak, Kuparuk and Prudhoe Bay field areas, North Slope, Alaska. Organic Geochem. 32 (3), 411–441.
Meng, B.K., Song, D.F., Chen, Y., Shi, S.B., 2024. Distribution and geochemical significance of alkylbenzenes for crude oil with different depositional environments and thermal maturities. Pet. Sci. 21 (2), 777–790.
Meng, B.K., Song, D.F., Chen, Y., Shi, S.B., 2025. New alkylbenzene parameters to identify organic matter sources for source rocks of light oils and condensates from the Tarim Basin and Beibuwan Basin. Pet. Sci. 22 (1), 76–89.
Milkov, A.V., 2011. Worldwide distribution and significance of secondary microbial methane formed during petroleum biodegradation in conventional reservoirs. Org. Geochem. 42 (2), 184–207.
Milkov, A.V., Etiope, G., 2018. Revised genetic diagrams for natural gases based on a global dataset of >20,000 samples. Org. Geochem. 125, 109–120.
Moldowan, J.M., Dahl, J., Zinniker, D., Barbanti, S.M., 2015. Underutilized advanced geochemical technologies for oil and gas exploration and production-1. The diamondoids. J. Pet. Sci. Eng. 126, 87–96.
Ni, Y.Y., Dai, J.X., Zou, C.N., Liao, F.R., Shuai, Y.H., Zhang, Y., 2013. Geochemical characteristics of biogenic gases in China. Int. J. Coal Geol. 113, 76–87.
Ni, C.H., Wu, X.Q., Wang, P., Wang, F.B., Jia, H.C., Zhu, J.H., Zhang, Y., Jiang, H.J., 2024. Geochemical characteristics of light hydrocarbons in Upper Paleozoic tight gas form Daniudi Gas Field, Ordos Basin. Petrol. Geol. Exp. 46 (2), 366–379 (In Chinese).
Obermajer, M., Osadetz, K.G., Fowler, M.G., Silliman, J., Hansen, W.B., Clark, M., 2002. Delineating compositional variabilities among crude oils from Central Montana, USA, using light hydrocarbon and biomarker characteristics. Org. Geochem. 33 (12), 1343–1359.
Odden, W., Patience, R.L., Van Graas, G.W., 1998. Application of light hydrocarbons (C_4–C_{13}) to oil/source rock correlations: a study of the light hydrocarbon compositions of source rocks and test fluids from offshore Mid-Norway. Org. Geochem. 28 (12), 823–847.
Pei, L.X., Liu, W.H., Guo, Q., Wang, X.F., Luo, H.Y., Wang, Q.T., 2023. Genetic significance of carbon isotope curve types of methane, ethane, and propane in natural gas. Org. Geochem. 186, 104691.
Peng, W.L., Liu, Q.Y., Hu, G.Y., Liu, Y., Zhu, D.Y., Meng, Q.Q., Guo, F.T., Wang, R.L., 2020. Mechanisms of carbon isotopic fractionation in the process of natural gas generation: Geochemical evidence from thermal simulation experiment. Pet. Explor. Dev. 47 (5), 1042–1054.
Peng, Y.Y., Cai, C.F., Fang, C.C., Wu, L.L., Liu, J.Z., Sun, P., Liu, D.W., 2022. Diamondoids and thiadiamondoids generated from hydrothermal pyrolysis of crude oil and TSR experiments. Sci. Rep. 12, 196.
Peters, K.E., Moldowan, J.M., McCaffrey, M.A., Fago, F.J., 1996. Selective biodegradation of extended hopanes to 25-norhopanes in petroleum reservoirs. Insights from molecular mechanics. Organic Geochem. 24 (8–9), 765–783.
Phillips, J.B., Beens, J., 1999. Comprehensive two-dimensional gas chromatography: a hyphenated method with strong coupling between the two dimensions. J. Chromatogr. A 856 (1–2), 331–347.
Piasecki, A., Sessions, A., Lawson, M., Ferreira, A.A., Santos Neto, E.V., Eiler, J.M., 2016a. Analysis of the site-specific carbon isotope composition of propane by gas source isotope ratio mass spectrometer. Geochim. Cosmochim. Acta 188, 58–72.
Piasecki, A., Sessions, A., Peterson, B., Eiler, J., 2016b. Prediction of equilibrium distributions of isotopologues for methane, ethane and propane using density functional theory. Geochim. Cosmochim. Acta 190, 1–12.
Piasecki, A., Sessions, A., Lawson, M., Ferreira, A.A., Santos Neto, E.V., Ellis, G.S., Lewan, M.D., Eiler, J.M., 2018. Position-specific ^{13}C distributions within propane from experiments and natural gas samples. Geochim. Cosmochim. Acta 220, 110–124.
Prinzhofer, A.A., Huc, A.Y., 1995. Genetic and post-genetic molecular and isotopic fractionations in natural gases. Chem. Geol. 126 (3–4), 281–290.
Prinzhofer, A., Mello, M.R., Takaki, T., 2000. Geochemical Characterization of Natural Gas: A Physical Multivariable Approach and its applications in Maturity and Migration estimates. AAPG Bull. 84 (8), 1152–1172.
Proskurowski, G., Lilley, M.D., Seewald, J.S., Fruh-Green, G.L., Olson, E.J., Lupton, J.E., Sylva, S.P., Kelley, D.S., 2008. Abiogenic hydrocarbon production at lost City hydrothermal field. Science 319 (5863), 604–607.
Qi, Y., Sun, P., Cai, C.F., Wang, D.W., Peng, Y.Y., 2022. Phase fractionation controlling regional distribution of diamondoids: A case study from the Halahatang oil field, Tarim Basin, China. Mar. Petrole. Geol. 140, 105674.
Qiao, R.Z., Chen, Z.H., 2022. Petroleum phase evolution at high temperature: A combined study of oil cracking experiment and deep oil in Dongying Depression, eastern China. Fuel 326 (15), 124978.
Qiao, R.Z., Chen, Z.H., Li, C.Y., Wang, D.Y., Gao, Y., Zhao, L.Q., Li, Y.Q., Liu, J.Y., 2022. Geochemistry and accumulation of petroleum in deep lacustrine reservoirs: A case study of Dongying Depression, Bohai Bay Basin. J. Pet. Sci. Eng. 213, 110433.
Qiao, R.Z., Li, M.J., Zhang, D.L., Xiao, H., 2024a. Geochemistry and accumulation of the ultra-deep Ordovician oils in the Shunbei oilfield, Tarim Basin: Coupling of reservoir secondary processes and filling events. Mar. Pet. Geol. 167, 106959.
Qiao, R.Z., Li, M.J., Zhang, D.L., Xiao, H., 2024b. Distribution and origin of higher diamondoids in the ultra-deep Paleozoic condensates of the Shunbei oilfield in the Tarim Basin. NW China. Organic Geochemistry 197, 104883.
Qiao, R.Z., Li, M.J., Zhang, D.L., Chen, Z.H., Xiao, H., 2024c. Evaporative fractionation as the important formation mechanism of light oil reservoirs in the dongying depression, NE China. Energies 17, 3734.
Qiao, R.Z., Li, M.J., Zhang, D.L., Xiao, H., 2025a. Enlightenment of geochemistry for ultra-deep petroleum accumulation: Coupling of secondary processes and filling events. Pet. Sci. 22, 1465–1484.
Qiao, R.Z., Li, M.J., Zhang, D.L., Xiao, H., Wang, W.Q., 2025b. Polycyclic aromatic compounds in crude oil as proxies for Permian Tarim large igneous province activities. Geosci. Front. 16 (2), 102000.
Qiu, N.S., Chang, J., Zhu, C.Q., Liu, W., Zuo, Y.H., Xu, W., Li, D., 2022. Thermal regime of sedimentary basins in the Tarim, Upper Yangtze and North China Cratons. China. Earth-Science Reviews 224, 103884.
Rabbani, A.R., Asemani, M., Kazemi, H., Nikandish, A., 2023. Application of light hydrocarbons for classification and geochemistry characterization of condensates from the Gavbendi High, Southwest Iran. Mar. Pet. Geol. 153, 106255.
Ricci, A., Cremonini, S., Severi, P., Tassi, F., Vaselli, O., Rizzo, A.L., Caracausi, A., Grassa, F., Fiebig, J., Capaccioni, B., 2023. Sources and migration pathways of methane and light hydrocarbons in the subsurface of the Southern Po River Basin (Northern Italy). Mar. Pet. Geol. 147, 105981.
Rice, D.D., 1992. Controls, habitat, resource potential of ancient bacterial gas. In: Vitaly, R. (Ed.), Bacterial Gas. Editions Technip, pp. 91–118.
Rice, D.D., Claypool, G.E., 1981. Generation, Accumulation, and Resource potential of Biogenic Gas. AAPG Bull. 65 (1), 5–25.
Rooney, M.A., Claypool, G.E., Moses Chung, H., 1995. Modeling thermogenic gas generation using carbon isotope ratios of natural gas hydrocarbons. Chem. Geol. 126 (3–4), 219–232.
Rosenfeld, W.D., Silvermann, S.R., 1959. Carbon Isotope Fractionation in Bacterial production of methane. Science 130, 1658–1659.
Schaefer, R.G., Littke, R., 1988. Maturity-related compositional changes in the low-molecular-weight hydrocarbon fraction of Toarcian shales. Org. Geochem. 13 (4–6), 887–892.
Schaefer, R.G., Welte, D.H., Pooch, H., 1984. Geochemistry of low molecular weight hydrocarbons in two exploration wells of the Elmworth gas field (Western Canada Basin). Org. Geochem. 6, 695–701.
Schaeffer, R.G., Leythaeuser, D., Weiner, B., 1978. Single-step capillary column gas chromatographic method for extraction and analysis of sub-parts per billion (10^9) amounts of hydrocarbons (C_2–C_8) from rock and crude oil samples and its application in petroleum geochemistry. J. Chromatogr. A 167, 355–363.
Schloemer, S., Krooss, B.M., 2004. Molecular transport of methane, ethane and nitrogen and the influence of diffusion on the chemical and isotopic composition of natural gas accumulations. Geofluids 4 (1), 81–108.
Schoell, M., 1980. The hydrogen and carbon isotopic composition of methane from natural gases of various origins. Geochim. Cosmochim. Acta 44 (5), 649–661.
Schoell, M., 1983. Genetic Characterization of Natural gases. AAPG Bull. 67 (12), 2225–2238.
Schulz, L.K., Wilhelms, A., Rein, E., Steen, A.S., 2001. Application of diamondoids to distinguish source rock facies. Org. Geochem. 32 (3), 365–375.
Shen, P., Sheng, Q.X., Wang, X.B., Xu, Y.C., 1987. Isotopiccomposition characteristics of gaseous hydrocarbons and identificationof coal type gas. Sci. Sin. Chim. 6, 647–656 (In Chinese).
Shurr, G.W., Ridgley, J.L., 2002. Unconventional shallow biogenic gas systems. AAPG Bull. 86 (11), 1939–1969.
Smith, M., Bend, S., 2004. Geochemical analysis and familial association of Red River and Winnipeg reservoired oils of the Williston Basin, Canada. Organic Geochem. 35 (4), 443–452.
Smith, J.T., Ehrenberg, S.N., 1989. Correlation of carbon dioxide abundance with temperature in clastic hydrocarbon reservoirs: relationship to inorganic chemical equilibrium. Mar. Pet. Geol. 6 (2), 129–135.
Snowdon, L.R., Powell, T.G., 1982. Immature oil and condensate: modification of hydrocarbon generation model for terrestrial organic matter. AAPG Bull. 66 (6), 775–788.
Song, D.F., Zhang, C.M., Li, S.M., Wang, T.G., Li, M.J., 2017. Elevated Mango's K1 Values Resulting from Thermochemical Sulfate Reduction within the Tazhong oils, Tarim Basin. Energy Fuels 31 (2), 1250–1258.

Srinivasan, P., Jacobi, D., Atwah, I., Karg, H., Azzouni, A., 2022. Generation temperatures for oils sourced from sulfur-rich kerogens using aromatic and light hydrocarbon isomers. Mar. Pet. Geol. 146, 105917.
Stahl, W., 1974. Carbon isotope fractionations in natural gases. Nature 251, 134–135.
Stahl, W.J., 1977. Carbon and nitrogen isotopes in hydrocarbon research and exploration. Chem. Geol. 20, 121–149.
Stahl, W.J., Carey, B.D., 1975. Source-rock identification by isotope analyses of natural gases from fields in the Val Verde and Delaware basins, west Texas. Chem. Geol. 16 (4), 257–267.
Stetter, K.O., Huber, R., Blöchl, E., Kurr, M., Eden, R.D., Fielder, M., Cash, H., Vance, I., 1993. Hyperthermophilic archaea are thriving in deep North Sea and Alaskan oil reservoirs. Nature 365, 743–745.
Stolper, D.A., Sessions, A.L., Ferreira, A.A., Santos Neto, E.V., Schimmelmann, A., Shusta, S.S., Valentine, D.L., Eiler, J.M., 2014. Combined ^{13}C–D and D–D clumping in methane: Methods and preliminary results. Geochim. Cosmochim. Acta 126, 169–191.
Stolper, D.A., Martini, A.M., Clog, M., Douglas, P.M., Shusta, S.S., Valentine, D.L., Sessions, A.L., Eiler, J.M., 2015. Distinguishing and understanding thermogenic and biogenic sources of methane using multiply substituted isotopologues. Geochim. Cosmochim. Acta 161, 219–247.
Sun, P.A., Wang, Y.C., Leng, K., Li, H., Ma, W.Y., Cao, J., 2016. Geochemistry and origin of natural gas in the eastern Junggar Basin, NW China. Mar. Pet. Geol. 75, 240–251.
ten Haven, H.L., 1996. Applications and limitations of Mango's light hydrocarbon parameters in petroleum correlation studies. Org. Geochem. 24 (10–11), 957–976.
Thompson, K.F.M., 1979. Light hydrocarbons in subsurface sediments. Geochim. Cosmochim. Acta 43 (5), 657–672.
Thompson, K.F.M., 1983. Classification and thermal history of petroleum based on light hydrocarbons. Geochim. Cosmochim. Acta 47 (2), 303–316.
Thompson, K.F.M., 1987. Fractionated aromatic petroleums and the generation of gas-condensates. Org. Geochem. 11 (6), 573–590.
Thompson, K.F.M., 2010. Aspects of petroleum basin evolution due to gas advection and evaporative fractionation. Org. Geochem. 41 (4), 370–385.
Tian, L.J., Hu, G.Y., Guo, J.H., Wang, X.M., He, F., Qi, X.N., Li, Z.S., Guo, C.Y., 2023. New insight into abiotic or biotic gas in deep reservoirs of the CL-I gas field in Songliao Basin (China) by light hydrocarbons associated with natural gas. Mar. Pet. Geol. 149, 106091.
Tissot, B., Califet-Debyser, Y., Deroo, G., Oudin, J.L., 1971. Origin and evolution of hydrocarbons in early Toarcian Shales, Paris Basin, France. AAPG Bull. 55 (12), 2177–2193.
Tranchida, P.Q., Aloisi, I., Mondello, L., 2022. Chapter Three–Heart–cutting and comprehensive multidimensional gas chromatography: basic principles. Compr. Anal. Chem. 96, 69–92.
Ungerer, P., Behar, F., Villalba, M., Heum, O.R., Audibert, A., 1988. Kinetic modelling of oil cracking. Org. Geochem. 13 (4–6), 857–868.
Wang, X., Zhang, M., 2008. Compositional and geochemical characteristics of light hydrocarbons for typical marine oils and typical coal-generated oils in China. Chin. J. Geochem. 27, 407–411.
Wang, T.G., He, F.Q., Li, M.J., Hou, Y., Guo, S.Q., 2004a. Alkyldibenzothiophenes: molecular tracers for filling pathway in oil reservoirs. Chin. Sci. Bull. 49, 2399–2404.
Wang, Z.R., Schauble, E.A., Eiler, J.M., 2004b. Equilibrium thermodynamics of multiply substituted isotopologues of molecular gases. Geochim. Cosmochim. Acta 68 (23), 4779–4797.
Wang, P.R., Zhang, D.J., Xu, G.J., Xiao, T.R., Song, F.Q., Cai, B., 2008. Geochemical features of light hydrocarbons of typical salt lake oils sourced from Jianghan Basin, China. Org. Geochem. 39, 1631–1636.
Wang, X.B., Guo, Z.Q., Tuo, J.C., Guo, H.Y., Li, Z.X., Zhuo, S.G., Jiang, H.L., Zeng, L.W., Zhang, M.J., Wang, L.S., Liu, C.X., Yan, H., Li, L.W., Zhou, X.F., Wang, Y.L., Yang, H., Wang, G., 2009. Abiogenic hydrocarbons in commercial gases from the Songliao Basin, China. Sci. China Ser. D Earth Sci. 52, 213–226.
Wang, H.T., Zhang, S.C., Weng, N., Li, W., Qin, S.F., Ma, W.L., 2012. Analysis of condensate oil by comprehensive two-dimensional gas chromatography. Pet. Explor. Dev. 39 (1), 132–138.
Wang, G.L., Shi, S.B., Wang, P.R., Wang, T.G., 2013. Analysis of diamondoids in crude oils using comprehensive two-dimensional gas chromatography/time-of-flight mass spectrometry. Fuel 107, 706–714.
Wang, G.L., Cheng, B., Wang, T.G., Simoneit, B.R.T., Shi, S.B., Wang, P.R., 2014. Monoterpanes as molecular indicators to diagnose depositional environments for source rocks of crude oils and condensates. Org. Geochem. 72, 59–68.
Wang, Y.P., Chang, X.C., Cheng, B., Shi, S.B., 2015a. Comparison of C_5-C_7 light hydrocarbons in Halahatang Ordovician oil analyzed by comprehensive 2-D and conventional Gas Chromatography. Nat. Gas Geosci. 26 (9), 1672–1926 (In Chinese).
Wang, X.F., Liu, W.H., Shi, B.G., Zhang, Z.G., Xu, Y.C., Zheng, J.J., 2015b. Hydrogen isotope characteristics of thermogenic methane in Chinese sedimentary basins. Org. Geochem. 83–84, 178–189.
Wang, D.W., Cai, C.F., Yun, L., Liu, J.Y., Sun, P., Jiang, Z.W., Peng, Y.Y., Zhang, H., Wei, T.Y., Pei, B.B., 2023. Controls on petroleum stability in deep and hot reservoirs: A case study from the Tarim Basin. Mar. Pet. Geol. 147, 106014.
Wang, Q.H., Deng, H.Y., Mo, T., Cheng, B., Wang, Y.P., Liao, Z.W., 2024a. Carbon and hydrogen isotopic compositions of C_7 hydrocarbons and their geochemical significance in light oils/condensates from the Kuqa Depression, Tarim Basin, NW China. Organic Geochem. 192, 104783.
Wang, Q., Hao, F., Zhou, S.Y., Xue, Y.A., Zou, H.Y., Liu, J.Z., 2024b. Oil cracking under closed-system pyrolysis: Implications for deep oil occurrence and related source determination. Mar. Pet. Geol. 166, 106928.
Warr, O., Young, E.D., Giunta, T., Kohl, I.E., Ash, J.L., Sherwood Lollar, B., 2021. High-resolution, long-term isotopic and isotopologue variation identifies the sources and sinks of methane in a deep subsurface carbon cycle. Geochim. Cosmochim. Acta 294, 315–334.
Warren, J., 2000. Dolomite: occurrence, evolution and economically important associations, 52, pp. 1–81.
Webb, M.A., Miller, T.F., 2014. Position-specific and clumped stable isotope studies: comparison of the Urey and path-integral approaches for carbon dioxide, nitrous oxide, methane, and propane. Chem. Eur. J. 118 (2), 467–474.
Wenger, L.M., Isaksen, G.H., 2002. Control of hydrocarbon seepage intensity on level of biodegradation in sea bottom sediments. Org. Geochem. 33 (12), 1277–1292.
Wever, H.E., 2000. Petroleum and Source Rock Characterization based on C_7 Star Plot results: examples from Egypt. AAPG Bull. 84 (7), 1041–1054.
Whiticar, M.J., 1999. Carbon and hydrogen isotope systematics of bacterial formation and oxidation of methane. Chem. Geol. 161 (1–3), 291–314.
Whiticar, M.J., Snowdon, L.R., 1999. Geochemical characterization of selected Western Canada oils by C_5-C_8 compound specific Isotope Correlation (CSIC). Org. Geochem. 30 (9), 1127–1161.
Wood, J.M., Euzen, T., Cesar, J., 2024. Influence of faults on late-stage migration of methane-rich gas in a major unconventional hydrocarbon accumulation: Montney Formation, western Canada. Mar. Pet. Geol. 164, 106857.
Wu, X.Q., Ni, C.H., Ma, L.B., Wang, F.B., Jia, H.C., Wang, P., 2024a. Tracing of natural gas migration by light hydrocarbons: A case study of the Dongsheng gas field in the Ordos Basin, NW China. Petrol. Explor. Develop. 51 (2), 307–319.
Wu, X.Q., Yang, J., Wang, P., Li, H.J., Chen, Y.B., Ni, C.H., Zeng, H.S., 2024b. Gas source of the Middle Jurassic Shaximiao Formation in the Zhongjiang large gas field of Western Sichuan Depression: Constraints from geochemical characteristics of light hydrocarbons. Energy Geosci. 5 (2), 100263.
Xia, X.Y., Gao, Y.L., 2024. Compound-specific, intra-molecular, and clumped C fractionations in the thermal generation and decomposition of ethane and propane: A DFT and kinetic investigation. Geochim. Cosmochim. Acta 375, 50–63.
Xiao, Q.L., Sun, Y.G., Zhang, Y.D., Chai, P.X., 2012. Stable carbon isotope fractionation of individual light hydrocarbons in the C_6–C_8 range in crude oil as induced by natural evaporation: Experimental results and geological implications. Org. Geochem. 50, 44–56.
Xie, Z.Y., Li, Z.S., Wei, G.Q., Li, J., Wang, D.L., Wang, Z.H., Dong, C.Y., 2016. Experimental research on the potential of sapropelic kerogen degradation gas and discrimination of oil cracking gas. J. Nat. Gas Geosci. 1 (6), 471–479.
Xie, Z.Y., Wei, G.Q., Li, J., Xu, L., Zhang, L., Li, J., Li, Z.S., Wu, S.J., Guo, Z.Q., Hao, A.S., 2021. Geochemical characteristics and accumulation pattern of gas reservoirs of the Sinian-Permian in Central Sichuan uplift zone, Sichuan Basin. China Petrol. Explor. 26 (6), 50–67 (in Chinese).
Xiong, Y.Q., Geng, A.S., 2000. Carbon isotopic composition of individual light hydrocarbons evolved from pyrolysis of source rocks from Ying–Qiong Basins, China. Mar. Petrol. Geol. 17 (9), 1041–1051.
Xu, Y.C., 1994. Theory and Application of Natural Gas Genesis (in Chinese). Science Press, Beijing, pp. 1–414.
Yang, S.R., Gang, W.Z., Cao, J.J., Liu, J.P., Gao, G., Dang, W.L., 2022. Geochemical characteristics, origin and carbon isotope reversal of the presalt natural gas in the lower Paleozoic Ordovician carbonates, Ordos Basin. China. Marine and Petroleum Geology 139, 105577.
Yin, X.Y., Zhang, Y.N., Liu, Q., Gilbert, A., Liu, F.X., Gao, C.H., Zhang, S.T., Ridley, M.K., Liu, Y., 2024. Position-specific and clumped isotope equilibria in propane: Ab initio calculations beyond the harmonic and Born-Oppenheimer approximations. Chem. Geol. 657, 122107.
Young, E.D., Rumble, D., Freedman, P., Mills, M., 2016. A large-radius high-mass-resolution multiple-collector isotope ratio mass spectrometer for analysis of rare isotopologues of O_2, N_2, CH_4 and other gases. Int. J. Mass Spectrom. 401, 1–10.
Young, E.D., Kohl, I.E., Sherwood Lollar, B., Etiope, G., Rumble III, D., Li, S., Haghnegahdar, M.A., Schauble, E.A., McCain, K.A., Foustoukos, D.I., Sutclife, C., Warr, O., Ballentine, C.J., Onstott, T.C., Hosgormez, H., Neubeck, A., Marques, J.M., Pérez-Rodríguez, I., Rowe, A.R., LaRowe, D.E., Magnabosco, C., Yeung, L.Y., Ash, J. L., Bryndzia, L.T., 2017. The relative abundances of resolved $^{12}CH_2D_2$ and $^{13}CH_3D$ and mechanisms controlling isotopic bond ordering in abiotic and biotic methane gases. Geochim. Cosmochim. Acta 203, 235–264.
Yu, C., Gong, D.Y., Huang, S.P., Liao, F.R., Sun, Q.W., 2014. Characteristics of Light Hydrocarbons of Tight gases and its Application in the Sulige Gas Field, Ordos Basin, China. Energy Explor. Exploitation 32 (1), 211–226.
Yu, S.J., Zhu, H.Q., Li, R., Yang, Y.T., Li, Q., 2017. Tracing natural gas migration by integrating organic and inorganic geochemical data: A case study of the Jurassic gas fields in western Sichuan Basin, SW China. Petrol. Explor. Develop. 44 (4), 582–594.
Yu, M., Gao, G., Liu, M., Ma, W.Y., Tian, A.Q., Fan, K.T., Guo, L.L.B., He, D., Zhang, Y.J., 2024. Hydrocarbon Generation Characteristics of Coal-measure Source Rocks and their Contribution to Natural Gas: A Case Study of Middle and lower Jurassic Targets from the Southern Junggar Basin margin. Acta Geologica Sinica (English Edition) 98 (5), 1270–1284.
Zhan, Z.W., Wang, G.X., Tian, Y.K., Zhan, X., Liang, T., Wang, Y.P., Zou, Y.R., Peng, P.A., 2023. Determination and petroleum geochemical significance of short-chain alkylbenzenes in lacustrine source rocks. Org. Geochem. 185, 104685.
Zhang, W.Z., Li, J.F., 2001. Study on oil and gas source in Ordos Basin. China Petroleum Explor. 6 (4), 28–36 (in Chinese).
Zhang, C.M., Li, S.T., Zhao, H.J., Zhang, J., 2005. Applications of Mango's light hydrocarbon parameters to petroleum from Tarim basin, NW China. Appl. Geochem. 20 (3), 545–551.
Zhang, N.Z., Snyder, G.T., Lin, M., Nakagawa, M., Gilbert, A., Yoshida, N., Matsumoto, R., Sekine, Y., 2021. Doubly substituted isotopologues of methane hydrate ($^{13}CH_3D$ and $^{12}CH_2D_2$): Implications for methane clumped isotope effects,

source apportionments and global hydrate reservoirs. Geochim. Cosmochim. Acta 315, 127–151.
Zhang, L., Li, Y., Jiang, W.M., Xiong, Y.Q., 2022. Position-specific carbon isotopic composition of thermogenic propane: Insights from pyrolysis experiments. Org. Geochem. 166, 104379.
Zhang, D.L., Li, M.J., Qiao, R.Z., Xiao, H., 2024. Applicability and Limitation of Aromatic Maturity Parameters in High-Maturity Oil from Ultradeep Reservoirs. Energy Fuel 38 (19), 18413–18430.
Zhao, H., Liu, C.J., Larson, T.E., McGovern, G.P., Horita, J., 2020. Bulk and position-specific isotope geochemistry of natural gases from the late cretaceous Eagle Ford Shale, South Texas. Mar. Pet. Geol. 122, 104659.
Zhu, Y.M., Zhang, C.M., 1999. Application of Mango˙s light hydrocarbon parameters in classification of oils from Tarim Basin. Geochimica 28 (1), 26–33 (In Chinese).
Zhu, Y.M., Weng, H.X., Su, A.G., Liang, D.G., Peng, D.H., 2005. Geochemical characteristics of Tertiary saline lacustrine oils in the Western Qaidam Basin, Northwest China. Appl. Geochem. 20 (10), 1875–1889.
Zhu, G.Y., Wang, H.T., Weng, N., Huang, H.P., Lian, H.B., Ma, S.P., 2013. Use of comprehensive two-dimensional gas chromatography for the characterization of ultra-deep condensate from the Bohai Bay Basin, China. Org. Geochem. 63, 8–17.
Zhu, G.Y., Zhang, Z.Y., Zhou, X.X., Li, T.T., Han, J.F., Sun, C.H., 2019. The complexity, secondary geochemical process, genetic mechanism and distribution prediction of deep marine oil and gas in the Tarim Basin, China. Earth Sci. Rev. 198, 102930.
Zhu, G.Y., Milkov, A.V., Li, J.F., Xue, N., Chen, Y.Q., Hu, J.F., Zhang, Z.Y., Chen, Z.Y., 2021a. Deepest oil in Asia: Characteristics of petroleum system in the Tarim basin, China. J. Pet. Sci. Eng. 199, 108246.
Zhu, X., Chen, J., Zhang, C., Wang, Y., Liu, K., Zhang, T., 2021b. Effects of evaporative fractionation on diamondoid hydrocarbons in condensates from the Xihu Sag, East China Sea Shelf Basin. Mar. Pet. Geol. 126, 104929.
Zhu, D.Y., Liu, Q.Y., Huang, X.W., Meng, Q.Q., Wang, J.B., Li, P.P., Jin, Z.J., 2025. Large-scale accumulation of abiotic gases associated with subduction and volcanic activities in rift basins in eastern China. Org. Geochem. 200, 104900.
Zumberge, J., Ferworn, K., Brown, S., 2012. Isotopic reversal ('rollover') in shale gases produced from the Mississippian Barnett and Fayetteville formations. Mar. Pet. Geol. 31 (1), 43–52.